HOKKAIDO UNIVERSITY

A study on design of heterogeneous step-index single-mode multi-core fibers with the standard cladding diameter of 125-μm

（標準クラッド外径異種ステップインデックス型シングルモードマルチコアファイバ設計に関する研究）

A dissertation submitted to the

Graduate School of Information Science and Technology
Hokkaido University

Yizhou Wang

Supervisor: Kunimasa Saitoh

Sapporo, Japan
February 2022

Abstract

In this work, we focus on designing heterogeneous step-index multi-core fibers (Hetero-SI-MCFs) with the standard cladding diameter of 125-μm, which enables the utilization of the existing optical cables, connector interfaces, and conventional optical components. To estimate the inter-core crosstalk (XT) in Hetero-SI-MCFs, an analytical expression with a particularly simple form is derived for the mode-coupling coefficients between non-identical step-index (SI) cores, which enables a quick estimation of the XT values. The analytical results are in good agreement with the results obtained by numerical simulations by finite-element method (FEM). Using the derived analytical expression, the feasibility of designing conventional Hetero-SI-MCFs with one-ring core layout in the standard 125-μm cladding diameter is discussed. We then propose a novel method of allocating the non-identical cores in heterogeneous MCFs (Hetero-MCFs), where the crosstalk and critical bending radius (R_{pk}) are improved as compared to that of Hetero-MCFs designed by the conventional method. We numerically reveal that the number of SI cores that incorporated in the standard cladding diameter can be further increased with the proposed method of core allocation. It is shown that the simple SI profile enables us to allocate 8 and 6 non-identical cores in the standard cladding diameter of 125-μm for the O- and C-bands, respectively, and the achieved sufficiently low XT values support hundreds of kilometers transmission of the QPSK format signal. It is also shown that the simple SI profile enables us to allocate 10 and 8 non-identical cores in the standard cladding diameter of 125-μm for the O- and C-bands, respectively, and the achieved XT values support several kilometers transmission of the QPSK format signal, which has the potential use in datacenter networks. In addition, we propose a relatively low refractive index trench layer which occupies the outermost part of the conventional fiber cladding enables us to suppress the loss of outer cores in MCFs. A new kind of novel Hetero-SI-MCF with outer trench (OT) layer is proposed for achieving high core multiplicity. The designed MCFs with the comparable optical transmission characteristics to the conventional single-mode single-core fibers have the potential application in the space-division multiplexing systems.

key words: *Standard cladding diameter, heterogeneous multi-core fiber, step-index profile, space division multiplexing, outer trench layer.*

Contents

1 *Chapter 1. Introduction*

Space division multiplexing (SDM) has been proposed to overcome the capacity limitation of the existing optical communication system over the conventional single-mode single-core fiber (SM-SCF) [1]. Multi-core fibers (MCFs), in which multiple cores are packed in a single-fiber cladding, have been studied intensively and regarded as a promising implementation of SDM transmission.

Many types of single-mode MCFs (SM-MCFs) and few-mode multicore fibers (FM-MCFs) have been proposed to increase core count or mode count [2]. FM-MCF is a promising scheme to scale up the spatial channel count (SCC) since it combines multiple modes and multiple cores. The inter-core crosstalk (XT), which leads to signal distortion, is a common issue in SM-MCFs and FM-MCFs because it limits the transmission distance, transmission capacity, and modulation format [4]. In FM-MCFs, XT between the highest order modes needs to be concerned because the XT between the highest order modes is larger than the XT among other combination of modes [5]. The differential mode delay (DMD), which represents the time difference between the fastest mode and the slowest mode in a core, is another one important issue for FM-MCFs, because a large DMD requires heavy signal processing for recovering the coupled signals [5]. It is required to suppress DMD for all cores within a certain range in FM-MCFs. Some FM-MCFs exceeded the SCC of 100: 108 with 3 modes × 36 cores [6], 114 with 6 modes × 19 cores [7]. However, FM-MCFs should overcome both issues of XT and DMD simultaneously. On the other hand, SM-MCFs have the great advantage of upgradability from the existing equipment and require no complex signal processing of optical multiple-input multiple-output (MIMO) [8], facilitating a simple implementation for SDM transmission.

The maximum core count of SM-MCFs was beyond 30 [2]. However, the cladding diameters are larger than the standard 125-μm cladding diameter in order to realize such large core count while maintaining sufficiently low XT. Since the mechanical reliability evidently degrades as the cladding diameter increases [9], the standard cladding diameter is preferable for use in the tight bend situations. It is also known that MCFs with the standard cladding diameter enable the utilization of the existing optical cables, connector interfaces, and conventional optical components [11]. In addition, the already mature splicing and cabling technologies utilized for conventional single-core fibers can be applied to fabricate MCFs with the same cladding diameter [10], effecting a reduction in the fabrication cost.

Eight-core SM-MCFs with the standard cladding dimeter of 125-μm have been presented in [10]. However, both MCFs are limited to operate at O-band, and trench-assisted (TA) core are employed.

Four-core SM-MCFs with the standard cladding dimeter have been reported in [13], the sufficiently low XT are also realized by TA profile and W-shape profile, so that the MCFs can be applied to full-band operation or long-haul transmission. To further suppress XT, cores with a low refractive index structure such as TA core [10], hole-assisted (HA) core [18], and rod-assisted (RA) core [19] are presented, their basic idea is to enhance the mode confinement or reduce the mode field overlap by these low refractive index area. However, because these structures are all micrometer-sized structures and a large amount of fluorine dopant is required during the fabrication process [12], the fabrication becomes complex and expensive. Thus, using the simple step-index (SI) core is effective in the reduction of fabrication cost. Four-core SM-MCFs with the simple SI profile have been presented in [11], which are the record core count of the SI profile in the standard cladding diameter. However, the XT of the reported SM-MCFs are relatively high for C-band operation.

So far, two types of MCFs have mainly been proposed for use in transmission. One is the homogeneous MCF (Homo-MCF), in which all the cores are identical [10]; another one is the heterogeneous MCF (Hetero-MCF) which contains non-identical cores [9]. As compared with identical cores, non-identical cores can be more closely packed in a limited cladding diameter because the slight differences in their core radii and core refractive indices can make XT go down drastically. Thus, using the simple heterogeneous SI cores is a potential means to achieve sufficiently low XT while reducing the fabrication complexity and cost.

Therefore, In this study, we focus on using the non-identical SI cores to design MCFs within the standard cladding diameter of 125-μm, which can be expected to further increase the core count as compared to the 125-μm cladding MCFs reported so far [10].

This dissertation is structured as follows:

In chapter 2, we derive an analytical expression for mode-coupling coefficients between non-identical SI cores, which has a particular simple form that can be easily calculated using mathematical tools. Next, we introduce the estimation of XT between non-identical cores, some equations are reviewed. We then verify the validity of the derived analytical expression, facilitating its application to the XT estimation in heterogeneous step-index multi-core fibers (Hetero-SI-MCFs). Lastly, using the derived analytical expression, the feasibility of designing the conventional Hetero-SI-MCFs within the 125-μm standard cladding diameter is discussed.

In chapter 3, we propose a novel core allocation to modify the conventional Hetero-SI-MCFs, where we shorten the outer cladding thickness (T_C) of those cores with higher core refractive index,

resulting the enlargement of core pitch (D) for achieving lower XT values. The improvements in the modified Hetero-SI-MCFs as compared to the conventional Hetero-SI-MCFs are discussed. Using the proposed core allocation, it has been shown that the standard cladding diameter supports six and eight-core with sufficiently low XT for long-haul transmission for C- and O-band, respectively, and it also supports eight and ten-core with acceptable XT for transmission of several kilometers for C- and O-band, respectively.

In chapter 4, we propose an outer trench (OT) layer to suppress the loss of outer cores in the conventional Hetero-SI-MCFs. OT layer has a relatively low refractive index as compared to the standard fiber cladding and occupies the outermost part region of the fiber cladding, which enables us to allocate cores to a relatively thin T_C, effecting in the enlargement of core pitch. Using the proposed OT layer, it has also been shown that the standard cladding diameter supports eight-core with sufficiently low XT for O-band transmission.

In chapter 5, summaries of this dissertation are presented.

2 *Chapter 2. Analytical expression for mode-coupling coefficient between non-identical step-index cores*

In general, to design MCFs, mode-coupling coefficients between the cores are required for estimating the average inter-core XT. Rigorous results can be obtained by numerical simulations. However, these are usually very time-consuming. Analytical expressions for the mode-coupling coefficients between non-identical cores have been reported in Refs. [22]. However, many of their results are derived using the coupled-mode theory or a complicated method, and their primary objective is to analyze the power transfer between non-identical cores. Moreover, the derived expressions have not been applied for designing MCFs.

As another method, a simple two-core coordinate system has been successfully applied to derive the mode-coupling coefficients between identical SI cores [25], and a particularly simple expression has been derived. A similar coordinate system has been applied to derive the mode-coupling coefficients between non-identical TA cores [26]. However, because the modified Bessel functions of the first kind in the exact electric field expressions of the inner cladding and trench region are ignored for simplifying their derived expression, a large error is seen in the mode-coupling coefficient when the trench region is relatively close to the core region [27]. To the best of our knowledge, the analytical expression for the mode-coupling coefficients between non-identical SI cores has not yet been formulated using the similar coordinate system, where the exact electric field expressions can be used and good accuracy can be expected.

Therefore, in this chapter, we first derive an analytical expression for the mode-coupling coefficients between identical SI cores by the similar two-core coordinate system. Then, we verify the validity of the derived expression, facilitating the estimation of the XT values in Hetero-SI-MCFs. Next, the feasibility of designing the conventional Hetero-SI-MCFs within the standard cladding diameter is discussed.

2.1. *Derivation of the analytical expression*

The mode-coupling coefficient with the overlap integral of electromagnetic fields is generally written as follows [25]:

$$\kappa_{12} = \frac{\omega\varepsilon_0 \int_{-\infty}^{\infty}\int_{-\infty}^{\infty}\left(N^2 - {N_2}^2\right)\boldsymbol{E_1^*}\cdot\boldsymbol{E_2}dxdy}{\int_{-\infty}^{\infty}\int_{-\infty}^{\infty}\boldsymbol{u_z}\cdot(\boldsymbol{E_1^*}\times\boldsymbol{H_1}+\boldsymbol{E_1}\times\boldsymbol{H_1^*})dxdy} = \frac{\omega\varepsilon_0 \int_0^{2\pi}\int_0^{a}({n_1}^2 - {n_0}^2)\boldsymbol{E_1^*}\cdot\boldsymbol{E_2}rdrd\theta}{4\boldsymbol{P}}, \quad (1)$$

where κ_{12} represents the mode-coupling coefficient from core 2 to core 1. The subscripts 1 and 2 in Eq. (1) denote the parameters for core 1 and core 2, respectively. ω is the angular frequency of the electromagnetic fields and ε_0 is the permittivity of vacuum. $\boldsymbol{E}$ and $\boldsymbol{H}$ stand for the electric and magnetic fields, respectively, * denotes the complex conjugate, and $\boldsymbol{u}_z$ represents the unit vector of the z-axis. The denominator of the original function can be written as $4\boldsymbol{P}$, where $\boldsymbol{P}$ refers to the total power flow in core 1. As illustrated in Fig. 1, $N^2(x, y)$ denotes the refractive index distribution in the entire coupled region, and $N_2^2(x, y)$ represents the refractive index distribution of core 2, which consist of core 2 and the cladding region. Thus, the difference in refractive index inside core 1 is expressed as ${n_1}^2 - {n_0}^2$, where n_1 and n_0 represent the refractive indices of core 1 and the cladding, respectively.

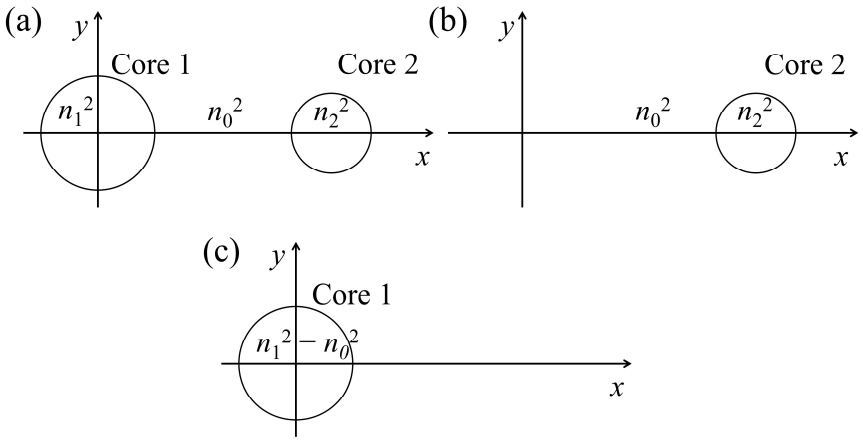

Fig. 1. Geometries for the calculation of κ_{12}. (a), (b), and (c) represent $N^2(x, y)$, $N_2^2(x, y)$, and $N^2(x, y) - N_2^2(x, y)$, respectively.

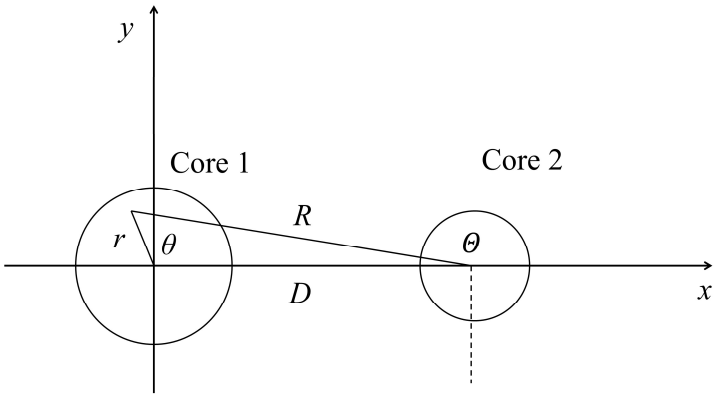

Fig. 2. Coordinate system for the calculation of κ_{12}. (R, Θ) is a coordinate system with its the origin at the center of core 2.

As illustrated in Fig. 2, to further simplify the numerator of Eq. (1), a coordinate system (R, Θ) whose origin is the center of core 2 is used, here D represents the core pitch. Hence, it is easy to consider the electric field in the core region of core 1 for $\boldsymbol{E}_1$ and the electric field in the cladding of core 2 for $\boldsymbol{E}_2$. The exact electric fields of the fundamental mode can be expressed by the following expressions [25].

Core region of core 1:

$$\begin{aligned} E_x &= C_1 J_0\left(\frac{U_1}{a_1} r\right) \cos\psi, \\ E_y &= -C_1 J_0\left(\frac{U_1}{a_1} r\right) \sin\psi, \\ E_z &= j\frac{U_1}{\beta_1 a_1} C_1 J_1\left(\frac{U_1}{a_1} r\right) \cos(\theta + \psi), \end{aligned} \tag{2}$$

Cladding region core 2:

$$\begin{aligned} E_x &= C_2 \frac{J_0(U_2)}{K_0(W_2)} K_0\left(\frac{W_2}{a_2} R\right) \cos\psi, \\ E_y &= -C_2 \frac{J_0(U_2)}{K_0(W_2)} K_0\left(\frac{W_2}{a_2} R\right) \sin\psi, \\ E_z &= j\frac{U_2}{\beta_2 a_2} C_2 \frac{J_1(U_2)}{K_1(W_2)} K_1\left(\frac{W_2}{a_2} R\right) \cos(\theta + \psi). \end{aligned} \tag{3}$$

As illustrated in Fig. 2, r denotes the distance from one point to the center of core 1 and R represents the distance from one point to the center of core 2. a_1 and a_2 denote the core radii of cores 1 and 2, respectively, U and W represent the normalized transverse wave numbers in the core and cladding region, respectively, and ψ denotes the phase. $J_n(z)$ represents the Bessel functions of the first

kind, and $K_n(z)$ represents the modified Bessel functions of the second kind, where $n = 0$ or 1 represents the order of the Bessel functions. C_1 and C_2 are related to the power flow $\boldsymbol{P}$ and are expressed by Eq. (4.111) in [25]:

$$C_1 = \frac{W_1}{a_1 V_1 J_1(U_1)}\sqrt{\frac{2\boldsymbol{P_1}}{\pi\varepsilon_0 n_1 c}},$$
$$C_2 = \frac{W_2}{a_2 V_2 J_1(U_2)}\sqrt{\frac{2\boldsymbol{P_2}}{\pi\varepsilon_0 n_2 c}}, \tag{4}$$

where c is the velocity of light in vacuum, and V is the normalized frequency.

Therefore, $\boldsymbol{E}^*_1 \cdot \boldsymbol{E}_2$ in Eq. (1) is expressed as follows:

$$E_1^* \cdot E_2 = C_1 C_2 J_0\left(\frac{U_1}{a_1}r\right)\frac{J_0(U_2)}{K_0(W_2)}K_0\left(\frac{W_2}{a_2}R\right) + \frac{U_1 U_2}{\beta_1\beta_2 a_1 a_2} C_1 C_2 J_1\left(\frac{U_1}{a_1}r\right)\frac{J_1(U_2)}{K_1(W_2)}K_1\left(\frac{W_2}{a_2}R\right)\cos(\theta+\psi)\cos(\Theta+\psi). \tag{5}$$

Because the second term on the right-hand side of Eq. (5) is sufficiently smaller than the first term, the integration term in the numerator becomes

$$S = \int_0^{2\pi}\int_0^a ({n_1}^2 - {n_0}^2) C_1 C_2 J_0\left(\frac{U_1}{a_1}r\right)\frac{J_0(U_2)}{K_0(W_2)}K_0\left(\frac{W_2}{a_2}R\right) r dr d\theta. \tag{6}$$

When $D >> r$, using the following approximation

$$R = \sqrt{D^2 + r^2 - 2Dr\cos\theta} \cong D - r\cos\theta, \tag{7}$$

and considering the case when the argument of the modified Bessel function $K_n(z)$ is large, it can be approximated as

$$K_n(z) \cong \sqrt{\frac{\pi}{2z}}\, exp(-z). \tag{8}$$

Therefore, using the following two integral formulas of Bessel functions:

$$I_0(z) = \frac{1}{\pi}\int_0^\pi \exp(z\cos\theta)d\theta, \tag{9}$$

$$\int_0^1 J_0(Uz) I_0(Wz) z dz = \frac{J_0(Uz)WI_1(Wz) + I_0(Uz)UJ_1(Wz)}{U^2 + W^2}, \tag{10}$$

the integration term of the numerator is further written as:

$$
\begin{aligned}
&S \\
&= 2\pi a_1^2 (n_1{}^2 \\
&- n_0{}^2) C_1 C_2 \frac{J_0(U_2)}{K_0(W_2)} \sqrt{\frac{\pi a_2}{2W_2 D}}\, exp\left(-\frac{W_2}{a_2} D\right) \frac{J_0(U_1) W_2 \frac{a_1}{a_2} I_1\left(U_2 \frac{a_1}{a_2}\right) + I_0\left(W_2 \frac{a_1}{a_2}\right) U_1 J_1(U_1)}{U_1{}^2 + \left(W_2 \frac{a_1}{a_2}\right)^2}
\end{aligned} \tag{11}
$$

where $I_n(z)$ represents the modified Bessel functions of the first kind.

Here, we consider that core 2 is not so much different from core 1, so that $C_2 \cong C_1$. The mode-coupling coefficient of core 2 to core 1 is finally given as follows:

$$
\begin{aligned}
&\kappa_{12} = \frac{\omega \varepsilon_0 S}{4\boldsymbol{P}} \\
&= \frac{\sqrt{\Delta_1}}{a_2} \frac{W_1 W_2}{V_2 J_1(U_1) J_1(U_2)} \sqrt{\frac{\pi a_2}{W_2 D}}\, exp\left(-\frac{W_2}{a_2} D\right) \frac{J_0(U_2)}{K_0(W_2)} \frac{J_0(U_1) W_2 \frac{a_1}{a_2} I_1\left(U_2 \frac{a_1}{a_2}\right) + I_0\left(W_2 \frac{a_1}{a_2}\right) U_1 J_1(U_1)}{U_1{}^2 + \left(W_2 \frac{a_1}{a_2}\right)^2},
\end{aligned} \tag{12}
$$

where Δ_1 is the relative core refractive index difference of core 1. By exchanging the subscripts 1 and 2 in Eq. (12), we obtain the mode-coupling coefficient from core 1 to core 2 (κ_{21}).

2.2. *Estimation of XT between two cores*

To easily estimate the XT in MCFs, coupled-power theory (CPT) has been introduced [28], [29]. The coupled power equations are written as [30]

$$
\frac{dP_m}{dz} = \sum_{n \neq m} h_{mn}[P_n(z) - P_m(z)], \tag{13}
$$

where P_m is the average power in core m and h_{mn} is the power coupling coefficient (PCC). The average power P_m in core m at a point z close to $z = 0$ is given by

$$
\begin{aligned}
P_m(z) &= \left\langle \left[K_{mn} A_n(0) \int_0^z \exp(j\beta'_{mn}\xi) \delta f(\xi)\, d\xi \right] \left[K_{mn} A_n^*(0) \int_0^z \exp(-j\beta'_{mn}\eta) \delta f^*(\eta)\, d\eta \right] \right\rangle \\
&= K_{mn}^2 P_n(0) \int_0^z d\eta \int_0^z \exp[j\Delta\beta'_{mn}(\xi - \eta)] \langle \delta f(\xi) \delta f^*(\eta) \rangle d\eta \\
&= K_{mn}^2 P_n(0) \int_0^z d\eta \int_{-\eta}^{z-\eta} \exp(j\Delta\beta'_{mn}\zeta) \langle \delta f(\eta + \zeta) \delta f^*(\eta) \rangle d\zeta,
\end{aligned} \tag{14}
$$

where the * and the symbol $\langle \quad \rangle$ indicate complex conjugation and an ensemble average, respectively. The random part of phase function, δf, is a stationary random process, it has an autocorrelation function $R(\zeta)$, and Eq. (14) can be rewritten as

$$P_m(z) = K_{mn}^2 P_n(0) z \int_{-\eta}^{z-\eta} \exp(j\Delta\beta'_{mn}\zeta) R(\zeta) d\zeta. \tag{15}$$

Since the two quantities, η and ζ, are not independent, it is difficult to evaluate the integral in Eq. (15). If the correlation length of δf, is much smaller than the increment z of fiber length, the bounds of the intergral can be neglected and replaced by $+\infty$ and $-\infty$, respectiely, therefore the PCC is finally written as [29]

$$h_{mn}(z) = \frac{P_m(z)}{zP_n(0)} = K_{mn}^2 S\left(\Delta\beta'_{mn}(z)\right), \tag{16}$$

where $S\left(\Delta\beta'_{mn}(z)\right)$ is the Fourier transform of the autocorelation function $R(\zeta)$. It has been reported that this autocorelation function can be well fitted by using exponential autocorrelation function [31] given by

$$R(\zeta) = \exp\left(-\frac{\zeta}{d}\right), \tag{17}$$

where d is the correlation length and its corresponding PCC is a Lorenzian function given by

$$h_{mn}(z) = \frac{2K_{mn}^2 d}{1 + [\Delta\beta'_{mn}(z)d]^2}. \tag{18}$$

When an MCF is bent at a constant radius and is twisted continuously, the PCC is averaged over a twist pitch as

$$\bar{h}_{mn} = \frac{\gamma}{2\pi} \int_0^{2\pi/\gamma} h_{mn}(z) dz, \tag{19}$$

where γ is a constant twist rate. Using the average PCC, the crosstalk XT between two cores with length L is easily estimated as [29]

$$\mathrm{XT} = \tanh\left(\bar{h}_{mn} L\right). \tag{20}$$

Notice that, in this case, the PCC is independent of the twist rate. From Eq. (18), we can find that PCC peaks at $\Delta\beta'_{mn} = 0$ at a particular bending radius. since $\Delta\beta'_{mn}$ is generally given by [29]

$$\Delta\beta'_{mn} = \Delta\beta_{mn} + \frac{\Lambda}{R}(\beta_m \cos\theta_m(z') - \beta_n \cos\theta_n(z')), \tag{21}$$

where Λ represents the distance between center of fiber cladding and core, R is the bending radius of a MCF, β_m and β_n are the propagation constants before the MCF getting bent in core m and core n, respectively. This particular critical bending radius (R_{pk}) is given by the following equation.

$$R_{\mathrm{pk}} = \frac{n_{eff}}{\Delta n_{eff,mn}} D, \tag{22}$$

where n_{eff} is the effective index of the mode, Δn_{eff} is the effective index difference between the core m

and core n, and D is the core pitch. in the case of homogeneous MCFs, where $\Delta\beta_{mn} = 0$, with small bending radii Eq. (18) can be approximated as

$$\bar{h}_{mn} = \frac{2K_{mn}^2 R}{\beta_m D}. \tag{23}$$

Here, the refined mode-coupling coefficient K_{mn} is the average value of mode-coupling coefficients κ_{12} and κ_{21} [29].

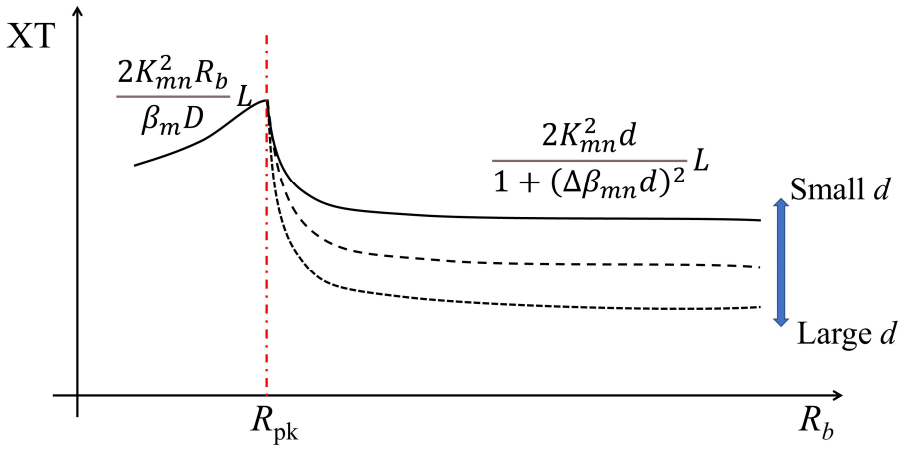

Fig. 3. Schematics of the XT in Hetero-MCFs.

Therefore, the schematics of the XT in Hetero-MCFs generally act as those depicted in Fig. 3. Because there is no phase-matching point along MCFs for $R_b > R_{pk}$, XT is given by Eq. (20) with Eq. (18) to evaluate the average PCC. In this region, the XT values decrease into an ultra-low value and varies with the correlation length d, a larger value of d yields a smaller value of XT. Thus, this region is generally considered as d-dominant [9]. In this study, d is assumed to be larger than 1 m for the estimation of XT because both the experimentally measured data and numerical results proved that the value of d between non-identical cores is larger than 1 m [2], [32].

On the other hand, in the phase-matching region where $R_b < R_{pk}$, XT is proportional to the bending radius and is independent on the correlation length d. The value of XT can be given by the Eq. (20) with Eq. (23) to evaluate the average PCC, and this region is generally considered as R-dominant [9].

2.3. *Validity of the analytical expression*

It is known that there is an effective core region (*ECR*) that is defined by the loss limits for designing MCFs [9]. Outside this region, cores with very large core radii or very high relative core refractive indices yield the higher-mode, whereas very small core radii or very low relative core refractive indices cause the loss of fundamental mode to be too large to be used. Therefore, in this section, we discuss the verification of the validity of the derived expression in the *ECR*. We compare the mode-coupling coefficients obtained by the derived analytical expression (K_{Ana}) with those obtained by FEM simulation (K_{FEM}) in the C- and O-bands, respectively. The comparison indicates that the error in the XT obtained by the analytical expression and FEM is less than 2.0 dB/km.

The error in K_{12} is simply defined as the ratio of K_{Ana} to K_{FEM}, as expressed by the following equation:

$$e_K = \frac{K_{\mathrm{Ana}}}{K_{\mathrm{FEM}}}. \tag{24}$$

Therefore, the difference between the XT values obtained by the analytical expression ($\mathrm{XT_{Ana}}$) and those obtained by FEM simulation ($\mathrm{XT_{FEM}}$) can be given by

$$\mathrm{XT_{diff}} = \mathrm{XT_{Ana}} - \mathrm{XT_{FEM}} = 10\log_{10}(e_K^2). \tag{25}$$

Owing to the strict loss requirements, it is easy to see that the largest core radius that can be used for C-band operation is approximately 4.9 μm with the highest relative core refractive index of approximately 0.42% from the Fig. 10 in Ref. [9], which also indicates that core 2 should have $a_2 \leq$ 4.9 μm with $\Delta_2 \leq 0.42\%$. Accordingly, we fix a_1 as 4.9 μm with $\Delta_1 = 0.42\%$ and change a_2 from 4.1 to 4.9 μm and Δ_2 from 0.34% to 0.42% to verify the validity.

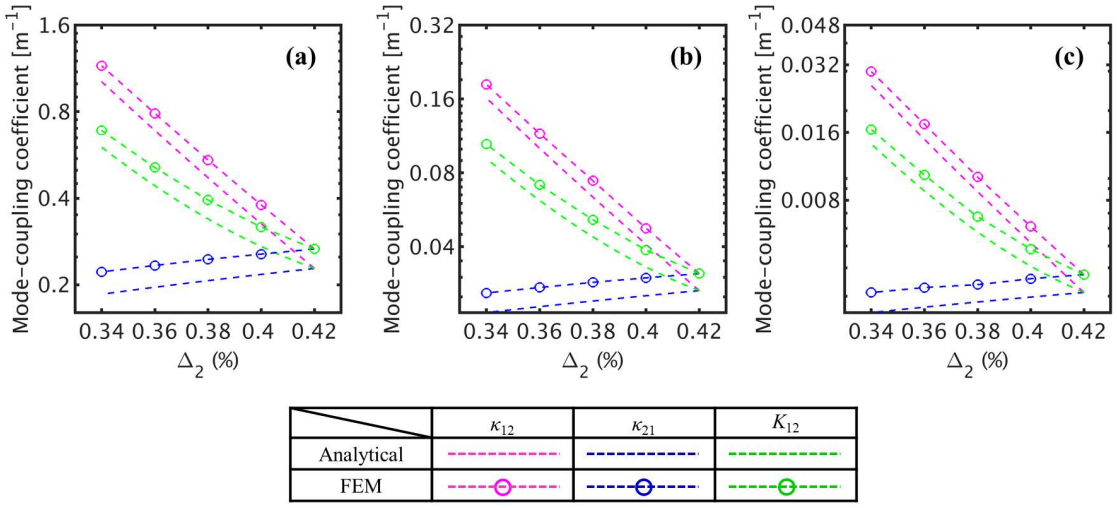

Fig. 4. Mode-coupling coefficients (κ_{12}, κ_{21}, and K_{12}) as functions of Δ_2 at λ = 1550 nm for D = (a) 30 μm, (b) 35 μm, and (c) 40 μm.

Figures 4 (a), (b), and (c) plot the mode-coupling coefficients (κ_{12}, κ_{21}, and K_{12}) as functions of Δ_2 at 1550 nm for D = 30, 35, and 40 μm, respectively, where $a_2 = a_1 = 4.9$ μm and Δ_2 ranges from 0.34% to 0.42%. The magenta, blue, and green dashed lines represent the analytical results of κ_{12}, κ_{21}, and K_{12}, respectively, and the magenta, blue, and green dashed lines with circles represent the FEM simulations of κ_{12}, κ_{21}, and K_{12}, respectively. We can see that the analytical results have the same trend as the FEM simulations. Due to the mode confinement becomes better, κ_{12} decreases as Δ_2 increases, whereas κ_{21} increases a little as Δ_2 increases because there is a small increase in the difference between the refractive indices. When $\Delta_2 = 0.42\%$, core 2 is identical to core 1, leading to $\kappa_{12} = \kappa_{21} = K_{12}$, which are represented by the rightmost green circles. Here, because the last term of Eq. (5) is ignored during the derivation, all the analytical results are smaller than those obtained by FEM simulations. The minimum value of e_K is 84% in Fig. 3, which is relatively high for a mode-coupling coeffecient. However, if we substitute this value into Eq. (25), the XT_{diff} can be expected to be less than 1.5 dB/km.

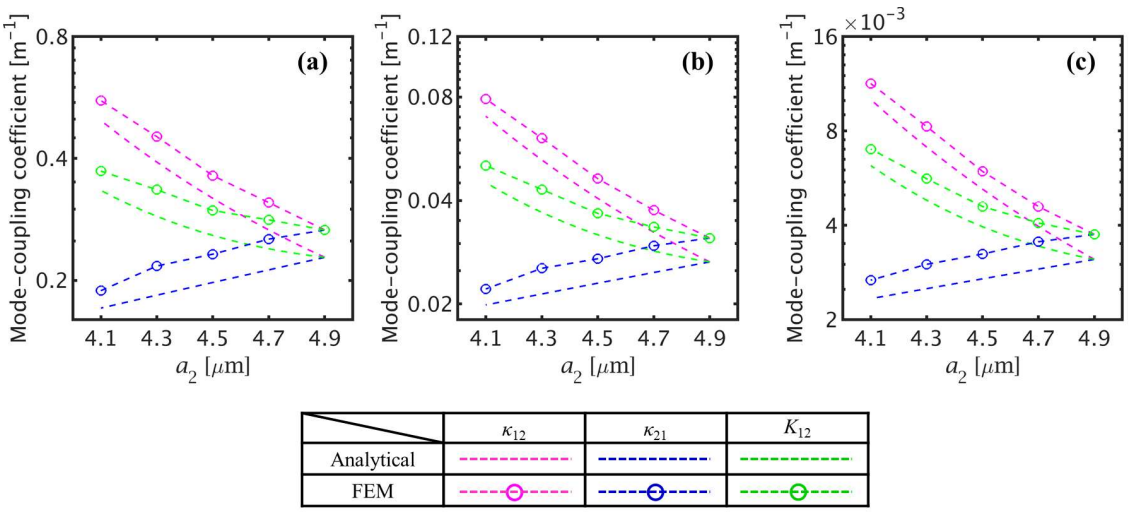

Fig. 5. Mode-coupling coefficients (κ_{12}, κ_{21}, and K_{12}) as functions of a_2 at λ = 1550 nm for D = (a) 30 μm, (b) 35 μm, and (c) 40 μm.

Figures 5 (a), (b) and (c) plot the mode-coupling coefficients as functions of a_2 at 1550 nm for D = 30, 35, and 40 μm, respectively, where $\Delta_2 = \Delta_1 = 0.42\%$ and a_2 ranges from 4.1 to 4.9 μm. We can also see high accuracy in the analytical results and FEM simulations, and κ_{12}, κ_{21}, and K_{12} show the same trend as that depicted in Fig. 4. The difference between K_{Ana} and K_{FEM} increases as the core radius increases because Eq. (7) is used in the derivation of the analytical expression, in the case of the fixed core pitch, it is more accurate when the core radius is small. Here, the minimum value of e_K is 84%, leading the value of $\mathrm{XT}_{\mathrm{diff}}$ to be less than 1.5 dB/km.

For the O-band operation, a_1 is fixed as 4.1 μm with $\Delta_1 = 0.39\%$ because this is the core parameter with the maximized optical confinement that can be operated along the O-band [5], and it also indicates that core 2 should have $a_2 \leq 4.1$ μm with $\Delta_2 \leq 0.39\%$. Here we consider that a_2 ranges from 3.3 to 4.1 μm and Δ_2 ranges from 0.31% to 0.39%.

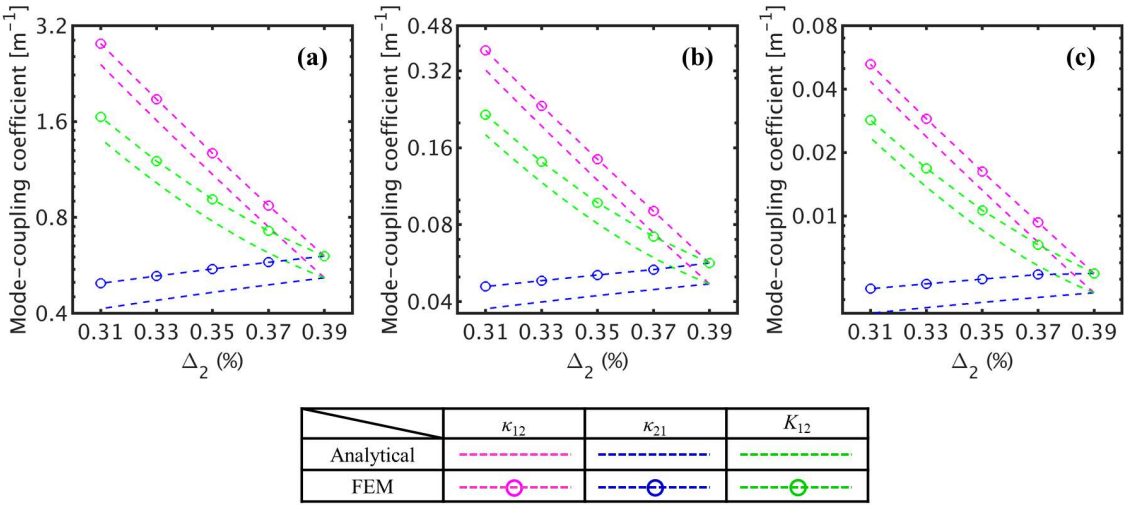

Fig. 6. Mode-coupling coefficients (κ_{12}, κ_{21}, and K_{12}) as functions of Δ_2 at λ = 1310 nm for D = (a) 25 μm, (b) 30 μm, and (c) 35 μm.

Figures 6 (a), (b), and (c) plot the mode-coupling coefficients as functions of Δ_2 at 1310 nm for D = 25, 30, and 35 μm, respectively, where $a_2 = a_1$ = 4.1 μm and Δ_2 ranges from 0.31% to 0.39%. We can also see that the analytical results indicate the same trend as the FEM simulations. The minimum value of e_K is 79%, which is relatively high for a mode-coupling coefficient. However, if we substitute this value into Eq. (25), the XT_{diff} can be expected to be less than 2.0 dB/km.

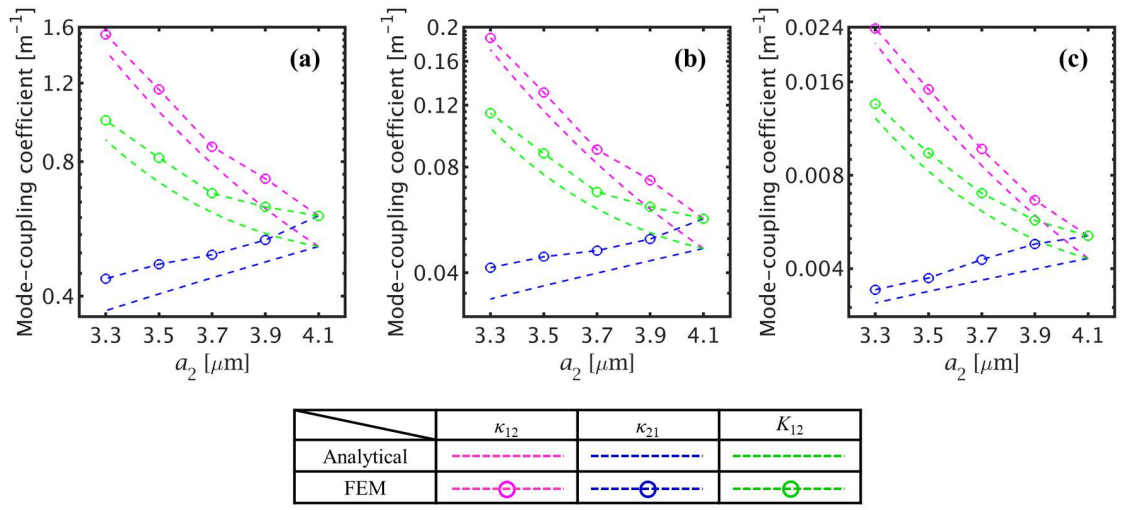

Fig. 7. Mode-coupling coefficients (κ_{12}, κ_{21}, and K_{12}) as functions of a_2 at λ = 1310 nm for D = (a) 25 μm, (b) 30 μm, and (c) 35 μm.

Figures 7 (a), (b), and (c) plot the mode-coupling coefficients as functions of a_2 at 1310 nm for D = 25, 30, and 35 μm, respectively, where $\Delta_2 = \Delta_1$ = 0.39% and a_2 ranges from 3.3 to 4.1 μm. We can also

see that the difference between K_{Ana} and K_{FEM} increases as the core radius increases, which can be attributed to the fact that Eq. (7) is more accurate for a smaller core radius when the core pitch is fixed. Here, the minimum value of e_K is 82%, leading the value of XT_{diff} to be less than 1.7 dB/km.

The error in the analytical expression is relatively high for evaluating mode-coupling coeffecient. However, the XT values obtained by the analytical expression are acceptable for evaluating the XT values between non-identical SI cores, which are considered to be 2.0 dB/km lower than those obtained by FEM simulations.

2.4. *Applications of the analytical expression*

2.3.1 Conventional Hetero-SI-MCFs for C-band

Reference [11] has reported that 125-μm cladding diameter supports four identical SI cores with XT of −28 dB/km at λ = 1550 nm. In this section, non-identical SI cores are adopted to increase the number of cores and suppress the XT in the C-band.

Heterogeneous core design means that the effective indices (n_{eff}s) are different for adjacent cores, the main target is to find cores with a large enough Δn_{eff}. To guarantee single-mode operation, cores are required to meet assumed loss requirements. The excessive loss (*EL*) which indicates the attenuation degradation of the outer cores due to macro-bending loss induced by high refractive index of fiber coating is one issue needs to be concerned [16]. It is pointed out that the refractive index of coating materials ($n_{coating}$) is a random value ranges from 1.465 to 1.485, which affects the loss of core [33]. However, since it is difficult to control the value of $n_{coating}$ in real fibers, the $n_{coating}$ is generally fixed as 1.486 in simulations [16]. In this study, all the $n_{coating}$ are also fixed as 1.486 in the evaluations of the loss of cores.

Selection of core parameters

Figures 8 (a) and (b) show the general method of core selections. Cores with different core radii (a) and relative refractive indices (Δ) have different effective areas (A_{eff}). For realizing the homogeneity of the transmission characteristics and low splice losses [9], cores with similar values of A_{eff} must be selected. For C-band use, we select cores with A_{eff} = 80 μm^2 at λ = 1550 nm, which is the general

recommendation for single-core single-mode fibers and is represented by the black dashed line.

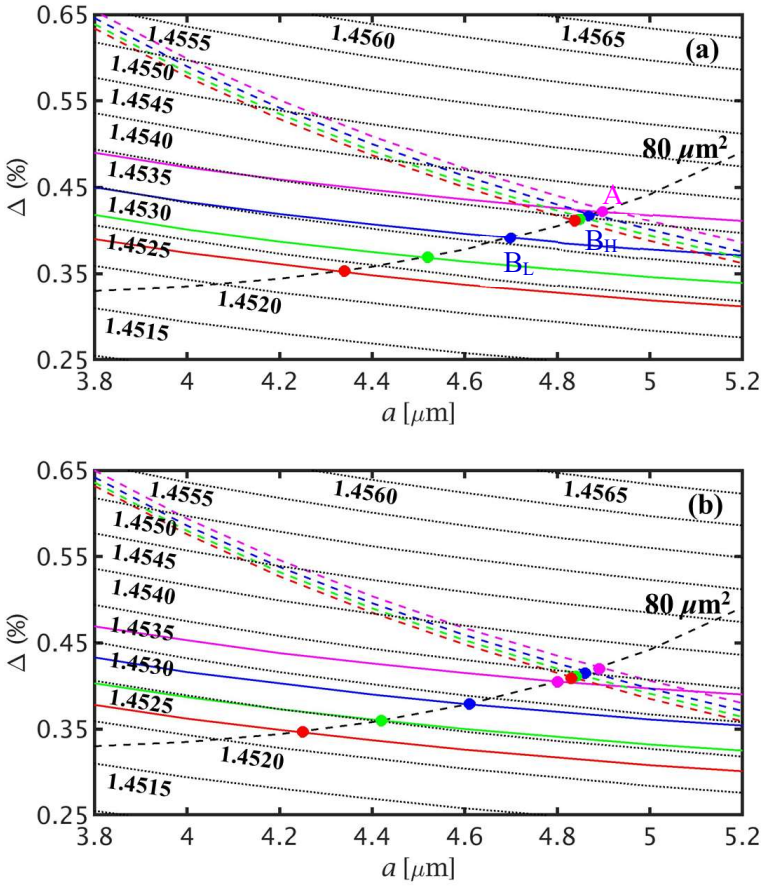

(a)	Cutoff limit	*EL* limit	(b)
T_C = 30 μm			T_C = 31 μm
T_C = 32 μm			T_C = 33 μm
T_C = 34 μm			T_C = 35 μm
T_C = 36 μm			T_C = 37 μm

Fig. 8. Relationship between the core parameters and effective indices for the C-band: (a) T_C = 30, 32, 34, and 36 μm; (b) T_C = 31, 33, 35, and 37 μm.

As the bending loss (*BL*) of the cores is strongly affected by the outer cladding thickness (T_C) [16], we start with a T_C of 30 μm and increase it in steps of 1 μm to select the cores for fiber design. To guarantee single-mode operation, the colored dashed lines represent the cutoff limits of LP_{11} mode for different values of T_C, which are plotted by assuming the *BL* of LP_{11} mode to be larger than 1 dB/m at λ = 1530 nm and R_b = 140 mm, whereas the colored solid lines represent the excessive loss (*EL*) limits of LP_{01} mode for different values of T_C, which are plotted by assuming the *BL* of LP_{01} mode to be less than 0.01 dB/km at λ = 1565 nm and R_b = 140 mm [11]. The black dotted lines represent the constant n_{eff}s

at λ = 1550 nm. These are all simulated based on full-vector FEM [34].

Based on these curves, it can be seen that only cores in the region surrounded by the dashed and solid lines of the same color and on the $A_{\mathrm{eff}} = 80\ \mu\mathrm{m}^2$ line are effective for fiber design. This region is termed as effective core region (*ECR*).

As shown in Fig. 8 (a), when $T_{\mathrm{C}} = 30\ \mu\mathrm{m}$, the *EL* limit, cutoff limit, and $A_{\mathrm{eff}} = 80\ \mu\mathrm{m}^2$ line intersect at the magenta dot, which indicates this core can be used to design homogeneous step-index MCFs (Homo-SI-MCFs) with a T_{C} of 30 μm. Furthermore, it is found that both the *EL* and cutoff limits are shifted to the lower core refractive region as T_{C} increases, and the *EL* limit descends more rapidly than the cutoff limit. This is because the loss of LP_{01} mode is more sensitive to T_{C} than that of LP_{11} mode, which leads to the enlargement of the *ECR*, facilitating the selection of non-identical cores to design Hetero-SI-MCFs.

Further, based on Eq. (22), a larger value of Δn_{eff} is able to achieve a smaller value of R_{pk}, which indicates that the XT will decrease to a low value more rapidly. Therefore, we use one core at the upper limit of *ECR* and another one core at the lower limit of *ECR* to design Hetero-SI-MCFs. For example, the two blue dots (cores $\mathrm{B_H}$ and $\mathrm{B_L}$) marked in Fig. 8 (a) are used for designing Hetero-SI-MCF with $T_{\mathrm{C}} = 32\ \mu\mathrm{m}$, and other dots of the same color marked in Fig. 8 (a) and (b) denote the core combinations for designing Hetero-SI-MCF with different values of T_{C}. Moreover, it is clear that all the cores are within the range verified in Section 2. 4, facilitating the estimation of the XT values by the derived expression directly.

Achievable XT

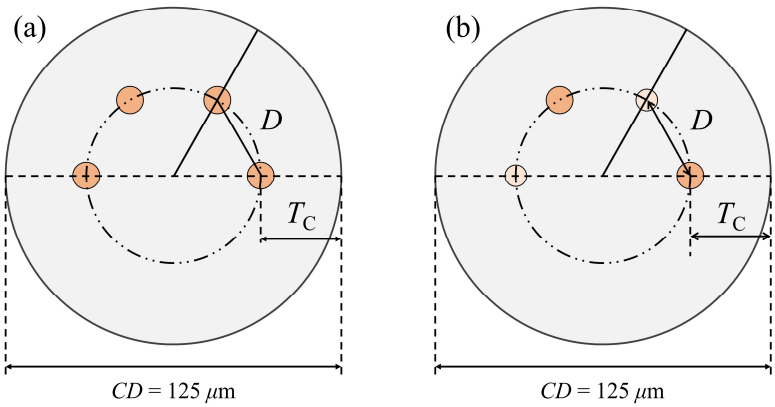

Fig. 9. Cross sections of the designed MCFs: (a) Homo-SI-MCFs with identical cores and (b) Hetero-SI-

MCFs with non-identical cores.

Owing to restricted loss requirements, the cores are required to be allocated as one-ring layout in the fiber cladding as shown in Fig. 9. When the number of cores (N_c) is determined, the core pitch can be easily calculated using the following equation.

$$D = 2(CD/2 - T_C)\sin(\pi/N_c), \tag{26}$$

where *CD* represents the cladding diameter and is fixed as 125 μm. Therefore, using Eq. (18), Eq. (20), and Eq. (23), the XT between two adjacent cores of the designed MCFs can easily be estimated.

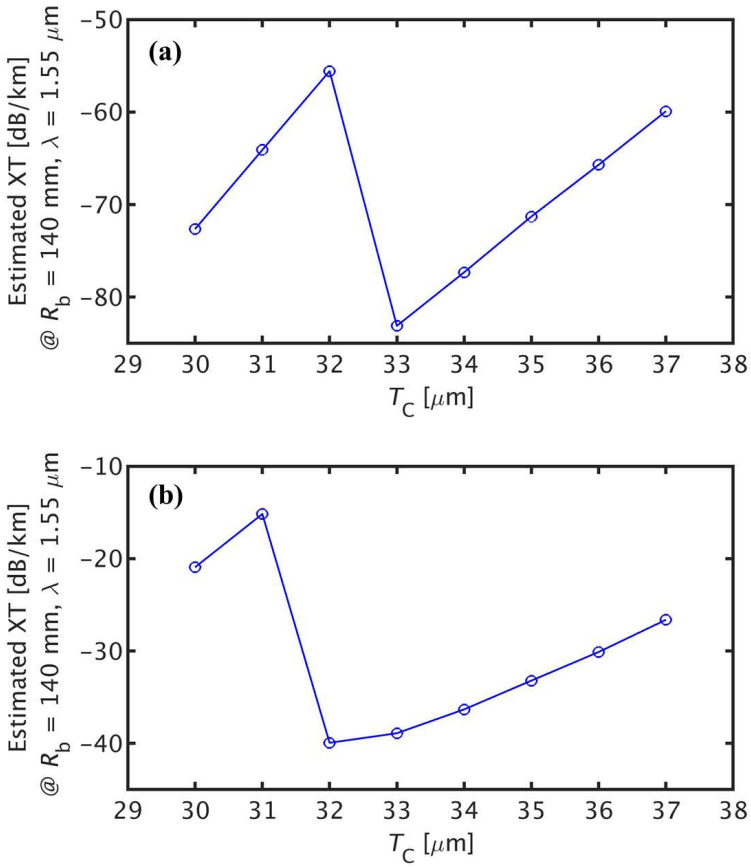

Fig. 10. Estimated nearest XT as functions of T_C for the C-band: (a) N_c = 4; (b) N_c = 6.

Figures 10 (a) and (b) plot the estimated nearest XT by the derived expression as functions of T_C for N_c = 4 and 6, respectively, in which the XT is estimated at λ = 1.55 μm and R_b = 140 mm, and *d* is assumed to be 1 m. When T_C = 30 μm, the XT of the Homo-SI-MCFs designed using the core A represented by the magenta dot marked in Fig. 8 (a) is plotted, when T_C > 30 μm, the XT of the Hetero-SI-MCFs designed using the core combinations represented by the dots of the same color depicted in

Fig. 8 (a) and (b) is plotted.

For N_c = 4, when T_C < 33 μm, the XT is relatively high because the R_{pk} of Hetero-SI-MCFs is larger than 140 mm. When T_C reaches 33 μm, the R_{pk} of Hetero-SI-MCFs is smaller than 140 mm, leading to a drastic decrease in the XT. Thereafter, the XT increases as T_C increases because K_{mn} increases rapidly as T_C increases. The best value of the nearest XT is −83.0 dB/km at T_C = 33 μm, because multiple cores are incorporated in one single-fiber cladding, we consider that the total XT for each core is equivalently caused by two neighboring cores, leading to a 3-dB/km increase in the total XT. In addition, considering a 2-dB/km increase in the XT owing to the error in the analytical expression, this four-core fiber has a total XT of −78.0 dB/km and can be expected to have negligible impact on the transmission performance [11]. In comparison with the four-core fiber reported in Ref. [11], the XT value is significantly improved.

For N_c = 6, when T_C < 32 μm, the XT is relatively high because the R_{pk} of Hetero-SI-MCFs is larger than 140 mm. When T_C reaches 32 μm, the XT drastically decreases into a low value because the R_{pk} of Hetero-SI-MCFs is smaller than 140 mm. The best value of the nearest XT is −39.7 dB/km at T_C = 32 μm. Considering a 2-dB/km increase in the XT owing to the error in the analytical expression and a 3-dB/km increase in it because of the two adjacent cores, the total XT value is −34.7 dB/km. Since it is already known that for a 1-dB XT penalty, the average XT levels of −16 dB are allowed for QPSK format signals [4], this six-core fiber can be expected to support the transmission of QPSK format signals with a XT penalty of 1 dB at approximately 70 km [4].

Therefore, for the C-band, by using the non-identical SI cores, the number of cores is increased by 2, and the XT value exceeds that of the Homo-SI-MCFs reported in Ref. [11].

2.3.2 Conventional Hetero-SI-MCFs for O-band

References [10] and [12] have reported eight-core fibers with 125-μm cladding diameter for O-band use. However, the sufficiently low XT is realized by TA profile. Here, we attempt to use the simple SI profile for easy fabrication. Furthermore, due to the overlap of TA structures, the number of cores reported in Refs. [10] and [12] reached the upper limit of 8. The simple SI cores facilitate a further increase in the number of cores within the limited diameter.

Selection of core parameters

For O-band use, T_C is initialized at 25 μm and increased to 32 μm in steps of 1 μm to select non-identical cores. The cutoff limits of LP_{11} mode are assumed to be larger than 1 dB/m at λ = 1260 nm and R_b = 140 mm, whereas the *EL* limits of LP_{01} mode are assumed be less than 0.01 dB/km at λ = 1310 nm and R_b = 140 mm [10]. The colored dashed and solid lines represent the cutoff and *EL* limits for the different values of T_C, respectively. The black dotted lines represent the constant n_{eff}s at λ = 1310 nm, and the black dashed line represents A_{eff} = 55 μm^2 at λ = 1310 nm, which is comparable to the effective area of the cores reported in Refs. [10].

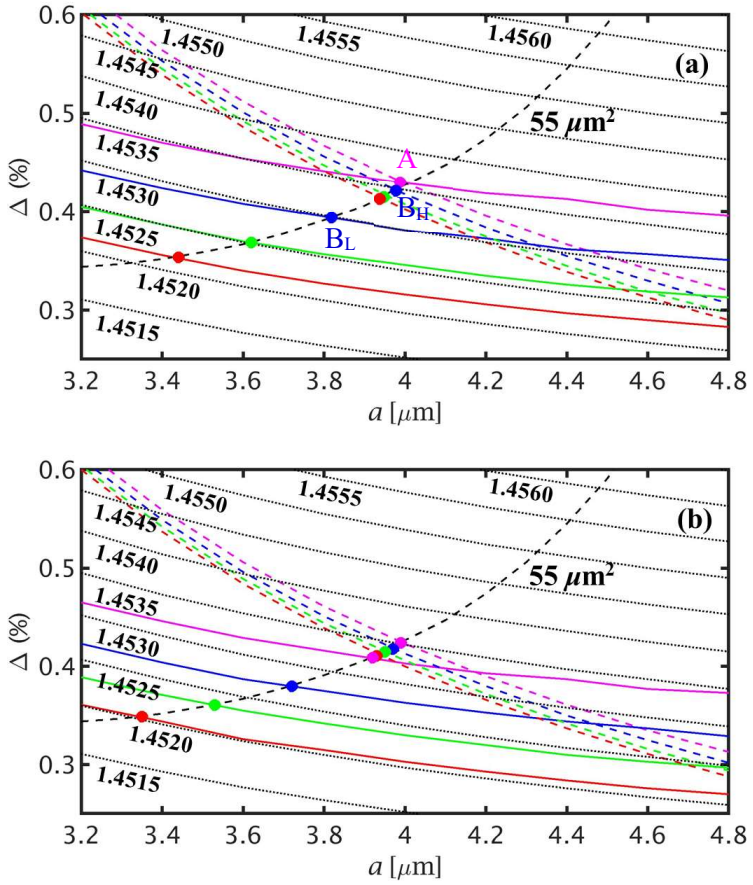

(a)	Cutoff limit	*EL* limit	(b)
T_C = 25 μm			T_C = 26 μm
T_C = 27 μm			T_C = 28 μm
T_C = 29 μm			T_C = 30 μm
T_C = 31 μm			T_C = 32 μm

Fig. 11. Relationship between the core parameters and effective indices for the O-band: (a) T_C = 25, 27, 29, and 31 μm; (b) T_C = 26, 28, 30, and 32 μm.

As shown in Fig. 11 (a), when T_C = 25 μm, the *EL* and cutoff limits intersect at the magenta dot at which A_{eff} = 54.6 μm^2. Although the value of A_{eff} is slightly less than the target of 55 μm^2, we use this core to design Homo-SI-MCFs. We can also find the enlargement of *ECR* as T_C increases, and the dots of the same color marked in Fig. 11 (a) and (b) are used for Hetero-SI-MCFs design. It is also clear that all the cores are within the range verified in Section 2. 4, facilitating the estimation of the XT values by the derived expression directly.

Achievable XT

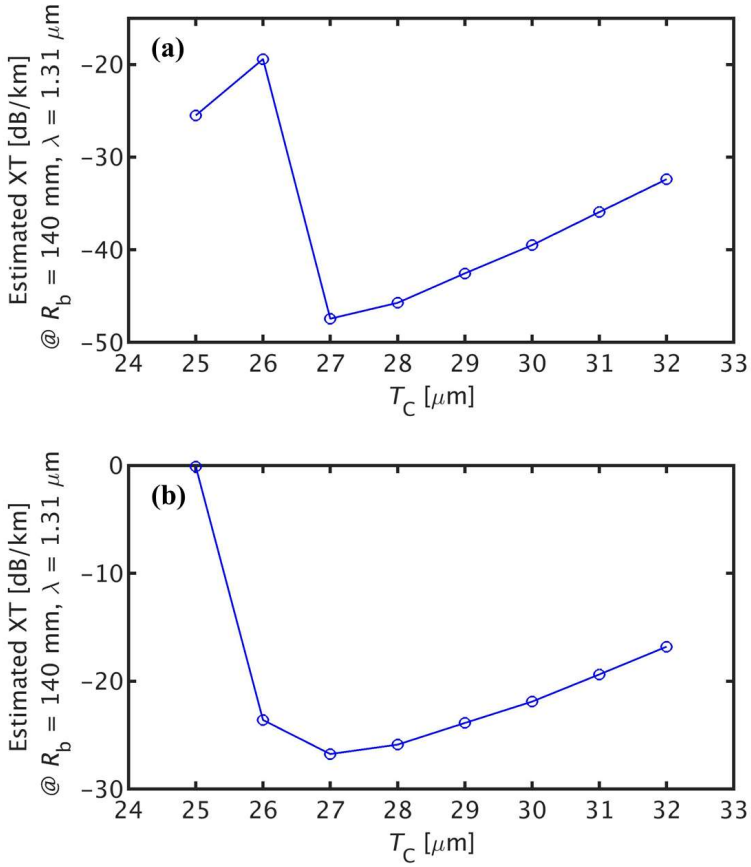

Fig. 12. Estimated nearest XT as functions of T_C for the O-band: (a) N_c = 8; (b) N_c = 10.

Figures 12 (a) and (b) plot the estimated nearest XT by the derived expression as functions of T_C for N_c = 8 and 10, respectively, where XT is estimated at λ = 1.31 μm and R_b = 140 mm, and d is assumed to be 1 m. When T_C = 25 μm, the XT of the Homo-SI-MCFs designed using the core represented by the magenta dot marked in Fig. 11 (a) is plotted. When T_C > 25 μm, the XT of the Hetero-SI-MCFs designed using the core combinations represented by the same color depicted in Fig.

11 (a) and (b) is plotted.

For N_c = 8, XT is relatively high when T_C < 27 μm. This is because the R_{pk} of Hetero-SI-MCFs is larger than 140 mm. When T_C reaches 27 μm, XT drastically decreases into a low value because the R_{pk} of Hetero-SI-MCFs is smaller than 140 mm. The best value of the nearest XT is −47.3 dB/km at T_C = 27 μm, yielding a total XT of −42.3 dB/km, this eight-core fiber can be expected to support at least hundreds of kilometers of transmission [4].

For N_c = 10, when T_C < 27 μm, XT is relatively high because the R_{pk} of Hetero-SI-MCF is larger than 140 mm. When T_C reaches 27 μm, XT decreases into a low value owing to the small R_{pk} of Hetero-SI-MCFs. The best value of the nearest XT is −26.6 dB/km at T_C = 27 μm, yielding a total XT of −21.6 dB/km, which can be expected to support the transmission of QPSK format signals over 3 km [4]. This is the first description of a ten-core fiber with 125-μm cladding diameter for O-band operation.

2.5. *Conclusion*

An analytical expression for the mode-coupling coefficient between non-identical SI cores is derived, which enables us to quickly estimate the XT values in Hetero-SI-MCFs without the need of numerical simulations. The derived analytical expression has a good accuracy as compared with the most rigorous numerical simulations by FEM. Therefore, it is a useful tool for the design of Hetero-SI-MCFs.

Using the derived analytical expressions, it has been shown that the simple SI profile enables us to allocate 10 and 6 non-identical cores in the 125-μm cladding diameter with the one-ring core layout for the O- and C-bands, respectively. The designed Hetero-SI-MCFs are shown in the following sections.

Designed conventional Hetero-SI-MCFs for C-band

The cross sections of the designed conventional four-core and six-core fibers for C-band are shown in Fig. 13 (a) and (b), respectively. Cores are allocated to the circle with T_C = 33 μm in the four-core fiber, while the cores are allocated to the circle with T_C = 32 μm in the six-core fiber.

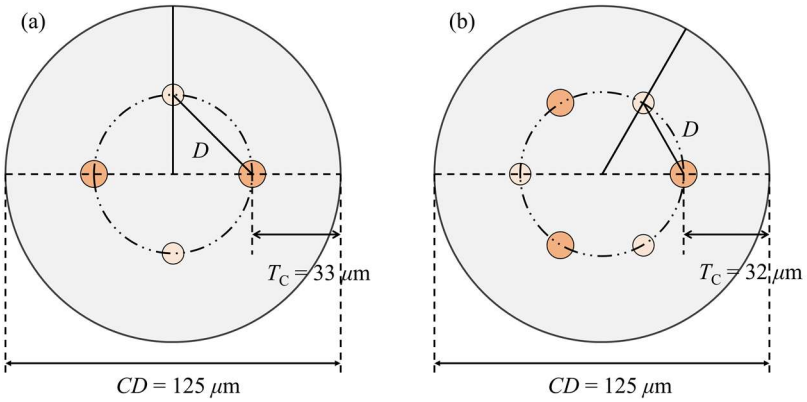

Fig. 13. Cross sections of the designed conventional Hetero-SI-MCFs for C-band. (a) 4-core fiber. (b) 6-core fiber.

The core parameters used for the designed conventional Hetero-SI-MCFs for C-band are listed in Table I, where core F_H is the one at the upper limit of *ECR*, and core F_L is the one at the lower limit of *ECR* for T_C = 33 μm, while core S_H is the one at the upper limit of *ECR*, and core S_L is the one at the lower limit of *ECR* for T_C = 32 μm. The main parameters of the designed conventioanl Hetero-SI-MCFs are listed in Table II.

Table. I Core parameters of the conventional modified Hetero-SI-MCFs for C-band.

Core number	a [μm]	Δ [%]	A_{eff} [μm^2]
F_H	4.86	0.415	80.1
F_L	4.61	0.379	80.1
S_H	4.87	0.417	80.0
S_L	4.70	0.391	80.0

Table. II Parameters of the designed conventional Hetero-SI-MCFs for C-band.

N_c	D [μm]	R_{pk} [mm]	XT [dB/km]
4	41.7	97.6	−78.0
6	30.5	99.8	−34.7

Figures 14 (a) and (b) plot the calculated nearest XT between the adjacent non-idnetical cores as functions of R_b for the designed four- and six-core fibers, respectively. XT is calculated at λ = 1550 nm, and d is assumed to be 1 m, 10 m, and 100 m, respectively. In both MCFs, the XT increases as R_b

increases in the *R*-dominant region, whereas the XT decreases into an ultra-low value and remains insensitive to R_b in the *d*-dominant region.

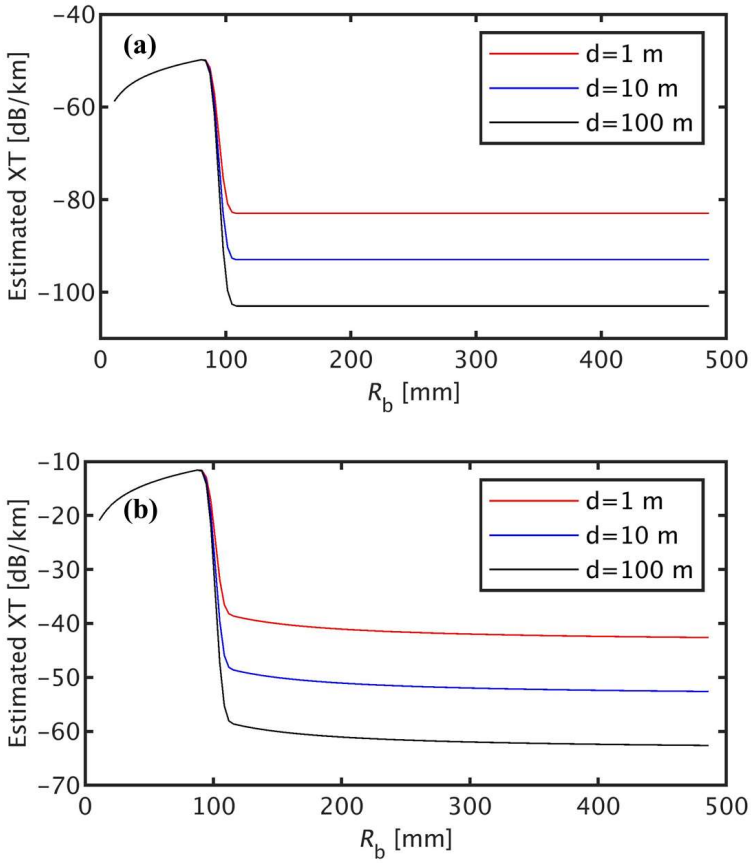

Fig. 14. Nearest XT between the adjacent cores in the designed conventional Hetero-SI-MCFs for C-band. (a) 4-core fiber. (b) 6-core fiber.

Designed conventional Hetero-SI-MCFs for O-band

The cross sections of the designed conventional eight-core and ten-core fibers for O-band are shown in Fig. 15 (a) and (b), respectively. in both cases, cores are allocated to the circle with $T_C = 27\ \mu$m.

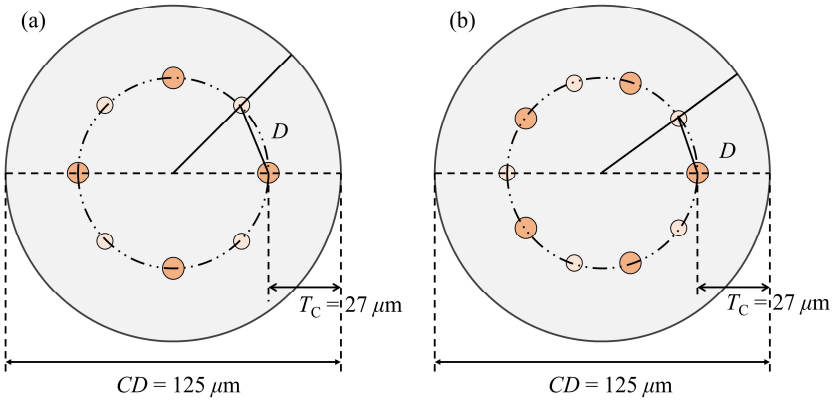

Fig. 15. Cross sections of the designed conventional Hetero-SI-MCFs for O-band. (a) 8-core fiber. (b) 10-core fiber.

The core parameters used for the designed conventional Hetero-SI-MCFs for O-band are listed in Table III. Core T_H is the one at the upper limit of *ECR*, and core T_L is the one at the lower limit of *ECR* for T_C = 27 μm, because both fibers have T_C = 27 μm, the core parameters are same. The main parameters of the designed conventioanl Hetero-SI-MCFs are listed in Table IV.

Table. III Core parameters of the conventional modified Hetero-SI-MCFs for O-band.

Core number	a [μm]	Δ [%]	A_{eff} [μm^2]
T_H	3.98	0.421	55.0
T_L	3.82	0.394	55.0

Table. IV Parameters of the designed conventional Hetero-SI-MCFs for O-band.

N_c	D [μm]	R_{pk} [mm]	XT [dB/km]
8	27.2	83.3	−42.3
10	21.9	67.3	−21.6

Figures 16 (a) and (b) plot the calculated nearest XT between the adjacent non-idnetical cores as functions of R_b for the designed eight- and ten-core fibers, respectively. XT is calculated at λ = 1310 nm, and d is assumed to be 1 m, 10 m, and 100 m, respectively. In both MCFs, the XT increases as R_b increases in the *R*-dominant region, whereas the XT decreases into an ultra-low value and remains insensitive to R_b in the *d*-dominant region. In Fig. 16 (b), the XT value of the designed ten-core fiber recheas 0 db/km at the *R*-dominant region.

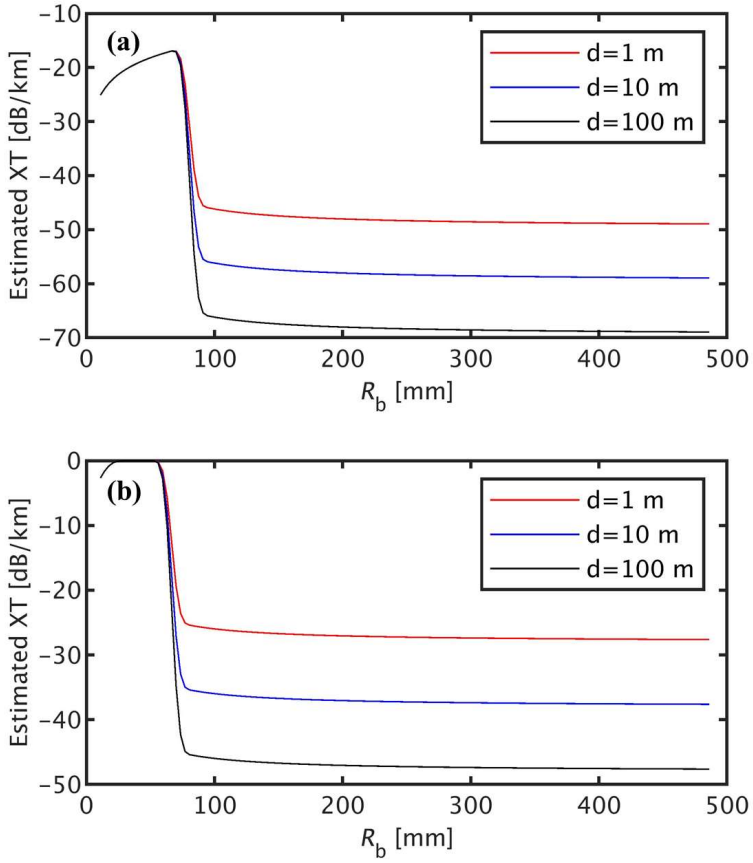

Fig. 16. Nearest XT between the adjacent cores in the designed conventional Hetero-SI-MCFs for O-band. (a) 8-core fiber. (b) 10-core fiber.

3 *Chapter 3. A novel core allocation for Hetero-MCFs*

3.1 Schematic of the proposed core allocation

The schematic of the proposed method of core allocation is shown in Fig. 17, where Fig. (a) shows the cross section of the conventional Hetero-MCFs with one-ring layout, where all the cores are equally allocated to a common circle whose center is the cladding center, which indicates all the cores have a common T_C, whereas Fig. (b) shows the cross section of the modified Hetero-MCFs, in which the cores with lower core refractive index and the cores with higher core refractive index are allocated to different circles respectively, because of the better core confinement, T_C of cores with higher core refractive index ($T_{C\text{-}H}$) could be smaller than that of cores with lower core refractive index ($T_{C\text{-}L}$), resulting the enlargement of core pitch (D) for achieving lower XT. Here, D_2 indicates the second nearest core pitch between the cores with lower core refractive index in the modified Hetero-MCFs. The steps to design the Hetero-SI-MCFs are introduced in the following sections.

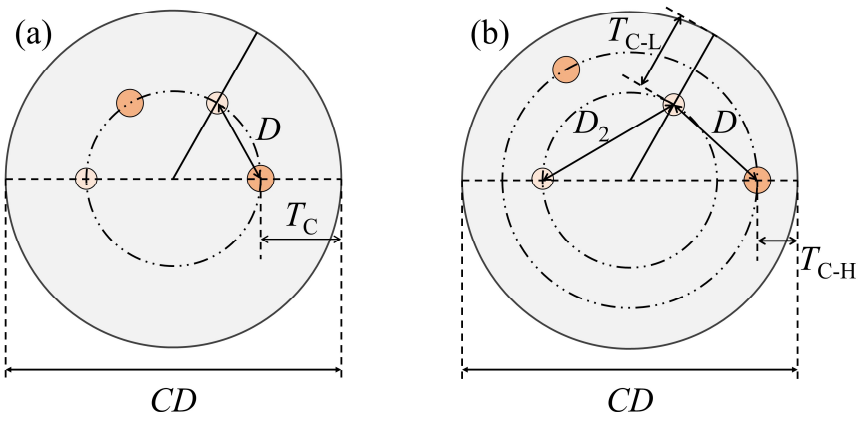

Fig. 17. Schematic of the proposed method for the Hetero-MCFs design. (a) Cross section of the conventional Hetero-MCFs. (b) Cross section of the modified Hetero-MCFs.

3.2 Applications of the proposed core allocation

In this section, the proposed method of core allocation is applied to fiber design for C- and O-band respectively, the improvements in critical bending radii (R_{pk}s) and XT values are discussed.

3.2.1. *Modified Hetero-SI-MCFs for C-band*

Here, we go back to Fig. 8 (a), where the core B_H and core B_L marked by blue dot are used as an example to introduce the difference between the conventional Hetero-MCF design and modified Hetero-MCF design in the case of T_C = 32 μm.

In the conventional Hetero-MCF design, core B_H and core B_L are allocated to the common circle with T_C = 32 μm, which indicates the $T_{C\text{-}L}$ = $T_{C\text{-}H}$ = 32 μm. However, in the modified Hetero-MCF design, core B_L is still allocated to the circle with $T_{C\text{-}L}$ = 32 μm, while core B_H is no longer lies at the upper limit of effective core region, because when the $T_{C\text{-}H}$ is reduced, the core A marked by the magenta dot can be allocated to the circle with T_C = 30 μm due to the shift-up of the cutoff limit line. Therefore, core A with $T_{C\text{-}H}$ = 30 μm is fixed in the modified Hetero-SI-MCFs, while the other one core is determined by $T_{C\text{-}L}$ and allocated to the circle with $T_{C\text{-}L}$. We should note that the core parameters will alter when $T_{C\text{-}L}$ changes, as shown by the other colored dots in Fig. 8 (a) and (b).

Since the XT of the conventional four-core fiber designed in the Section 2. 4 is already at extremely low value of −78 dB/km, we start with six-core fiber to discuss the improvements owing to the proposed method, and attempt to increase the number of cores that can be incorporated in the standard cladding diameter.

Improvement in R_{pk}s

With the reduction of $T_{C\text{-}H}$, it is easy to know that core pitch is enlarged, which is preferable for achieving a lower XT. However, according to Eq. (22), a larger core pitch yields a larger value of R_{pk}, while the change of higher refractive index core leads to the enlargement of Δn_{eff}, resulting a smaller value of R_{pk}. Therefore, in this section, we first discuss whether the proposed method enables us to improve the R_{pk}.

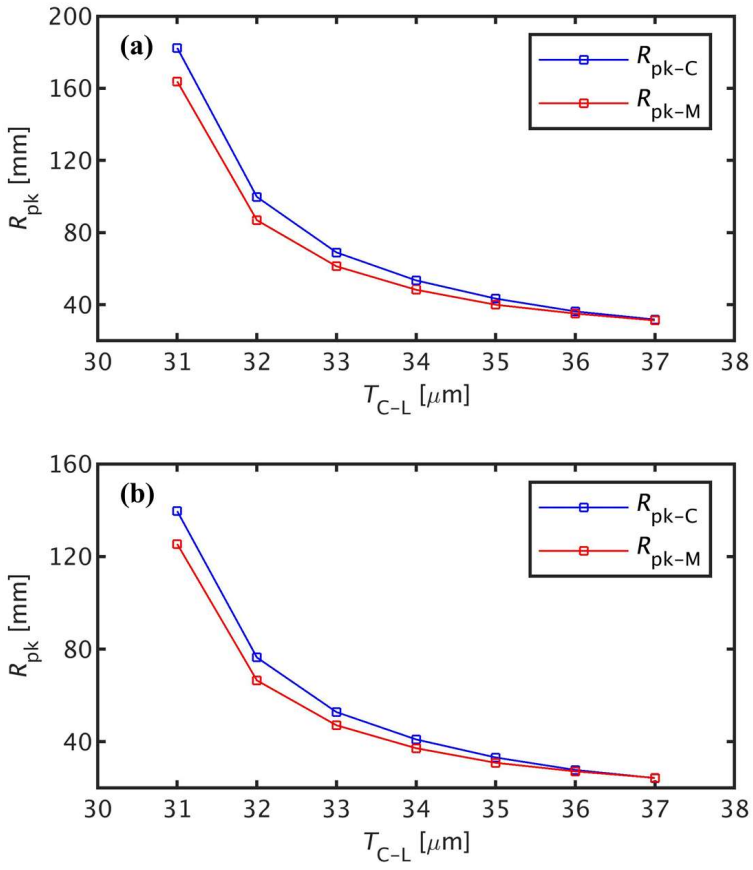

Fig. 18. Calculated R_{pk}s as functions of $T_{C\text{-}L}$ for C-band use: (a) $N_c = 6$; (b) $N_c = 8$.

Figures 18 (a) and (b) plot the critical bending radius of conventional Hetero-SI-MCFs ($R_{pk\text{-}C}$) and the critical bending radius of modified Hetero-SI-MCFs ($R_{pk\text{-}M}$) as functions of $T_{C\text{-}L}$ for N_c = 6 and 8, respectively. When $T_{C\text{-}L}$ equals to 30 μm, we use core A (the magenta dot in Fig. 8 (a)) to design Homo-SI-MCFs, so there is no critical bending radius plotted in Figs. 18 (a) and (b). When $T_{C\text{-}L}$ reaches 31 μm, the R_{pk}s of the designed Hetero-MCFs can be easily calculated by Eq. (22). It is clear that $R_{pk\text{-}M} < R_{pk\text{-}C}$ in all the cases, which indicates that the proposed method enables us to improve the R_{pk} of Hetero-SI-MCFs. We then turn to estimate the XT.

Improvement in XTs

Here, we plot the XT values calculated using the analytical expression derived (XT_{Ana}) in Section 2. 1, as well as the XT values calculated using FEM simulations (XT_{FEM}), where we can see the good accuracy of the derived expression for estimating the XT in Hetero-SI-MCFs.

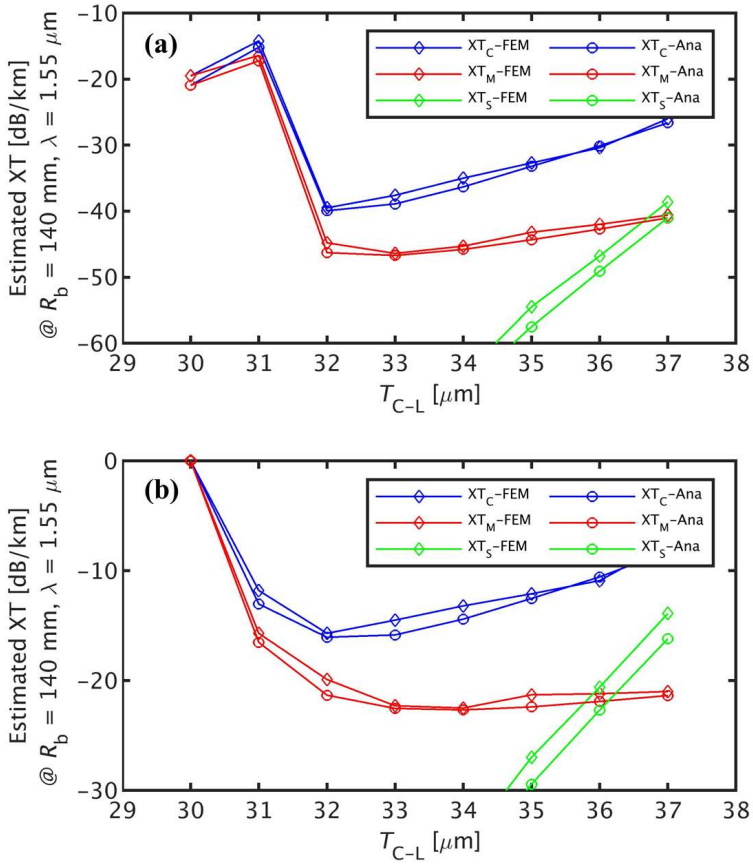

Fig. 19. Calculated XTs as functions of $T_{C\text{-}L}$ for C-band use: (a) $N_c = 6$; (b) $N_c = 8$.

Figures 19 (a) and (b) plot the estimated nearest XT of conventional Hetero-SI-MCFs (XT_C), nearest XT of modified Hetero-SI-MCFs (XT_M), and second nearest XT between the cores with lower core refractive index in modified Hetero-SI-MCFs (XT_S) as functions of $T_{C\text{-}L}$, where XTs are calculated at R_b = 140 mm and λ = 1550 nm, and d is assumed to be 1 m. When T_C = 30 μm, the XT of the Homo-SI-MCFs designed using the core A represented by the magenta dot marked in Fig. 8 (a) is plotted, so $XT_C = XT_M$. When T_C > 30 μm, the XT_C of the conventional Hetero-SI-MCFs designed using the core combinations represented by dots of the same color depicted in Fig. 8 (a) and (b) is plotted, whereas the XT_M of the modified Hetero-SI-MCFs designed using the core A in Fig. 8 (a) and the core at the lower limit of *ECR* for different values of $T_{C\text{-}L}$ is plotted.

For N_c = 6, when $T_{C\text{-}L}$ equals to 31 μm, because the R_{pk}s of Hetero-MCFs are larger than 140 mm, both the XT_C and XT_M are relatively large values of the *R*-dominant region, which indicates that a large enough Δn_{eff} is necessary to ensure R_{pk} to be smaller than a certain value. When $T_{C\text{-}L}$ reaches 32

μm, the R_{pk} of Hetero-MCFs is smaller than 140 mm, so both the XT_C and XT_M decease into ultra-low values of the *d*-dominant region.

In the conventional Hetero-SI-MCFs, XT_C increases as the $T_{C\text{-}L}$ increases, while in the modified Hetero-SI-MCFs, XT_M shows the best value at $T_{C\text{-}L}$ = 33 μm. Thereafter, the XT_M increases as $T_{C\text{-}L}$ increases. Here, according to the Eq. (22) in Ref. [31], since both the K_{mn} and $\Delta\beta_{mn}$ increases as $T_{C\text{-}L}$ increases, there is a tradeoff between them. In the conventional Hetero-SI-MCFs, we consider that K_{mn} is the dominant parameter, resulting the increase of XT_C, while in the modified Hetero-SI-MCFs, the region of $T_{C\text{-}L}$ < 33 μm is $\Delta\beta_{mn}$-dominant, which leads to the decrease of XT_M, and the region of $T_{C\text{-}L}$ > 33 μm is K_{mn}-dominant, resulting the increase of XT_M. Accordingly, we propose the modified six-core fiber with $T_{C\text{-}L}$ = 33 μm from the perspective of the best nearest XT_M value of −47.5 dB/km, considering a 3-dB/km increase in the total XT value because of the two adjacent cores, this XT_M value yields a total XT value of −44.5 dB/km and can be expected to support the transmission of QPSK format signals with a XT penalty of 1 dB over at least hundreds of kilometers [4].

The XT_S increases rapidly as $T_{C\text{-}L}$ increases and exceeds XT_M at $T_{C\text{-}L}$ = 37 μm, here, because XT_s is smaller than −60 dB/km for $T_{C\text{-}L}$ < 35 μm, that part of the green line is removed from Fig. 17 (a).

For N_c = 8, XT_C shows the best value at $T_{C\text{-}L}$ = 32 μm, thereafter, the XT_C increases as $T_{C\text{-}L}$ increases, while in the modified Hetero-SI-MCFs, XT_M shows the best value at $T_{C\text{-}L}$ = 34 μm, thereafter, the XT_M also increases as $T_{C\text{-}L}$ increases. Here, also according to the Eq. (22) in Ref. [31], we consider that for the conventional Hetero-SI-MCFs, the region of $T_{C\text{-}L}$ < 32 μm is $\Delta\beta_{mn}$-dominant, which leads to the decrease of XT_C, and the region of $T_{C\text{-}L}$ > 32 μm is K_{mn}-dominant, resulting the increase of XT_C. While for the modified Hetero-SI-MCFs, the region of $T_{C\text{-}L}$ < 34 μm is $\Delta\beta_{mn}$-dominant, which leads to the decrease of XT_M, and the region of $T_{C\text{-}L}$ > 34 μm is K_{mn}-dominant, resulting the increase of XT_M. Accordingly, we propose the modified eight-core fiber with $T_{C\text{-}L}$ = 34 μm from the perspective of the best nearest XT_M value of −23.4 dB/km, which yields a total XT value of −20.4 dB/km and can be expected to support the transmission of QPSK format signals with a XT penalty of 1 dB at approximately 3 km [4].

The XT_S increases rapidly as $T_{C\text{-}L}$ increases and exceeds XT_M at $T_{C\text{-}L}$ = 36 μm, because XT_s is smaller than −30 dB/km for $T_{C\text{-}L}$ < 35 μm, that part of the green line is removed from Fig. 17 (b).

From Figs. 17 (a) and (b), it is clear that XT_M < XT_C in all the cases, which indicates that the proposed method enables us to improve the XT of Hetero-SI-MCFs.

3.2.2. *Modified Hetero-SI-MCFs for O-band*

For O-band design, we go back to Fig. 11 (a), same as the Section 3.2.1, the core B_H and core B_L marked by blue dot are used as an example to introduce the difference between the conventional Hetero-MCF design and modified Hetero-MCF design in the case of $T_C = 27$ μm.

In the conventional Hetero-MCFs, the core B_H and core B_L are allocated to the common circle with $T_C = 27$ μm, whereas in the modified Hetero-MCF, the core A is fixed to the circle with $T_{C\text{-}H} = 25$ μm, and the other one core is determined by $T_{C\text{-}L}$ and allocated to the circle with $T_{C\text{-}L}$. We should note that the core parameters will alter when $T_{C\text{-}L}$ changes, as shown by the other colored dots in Fig. 11 (a) and (b).

Improvement in R_{pk}s

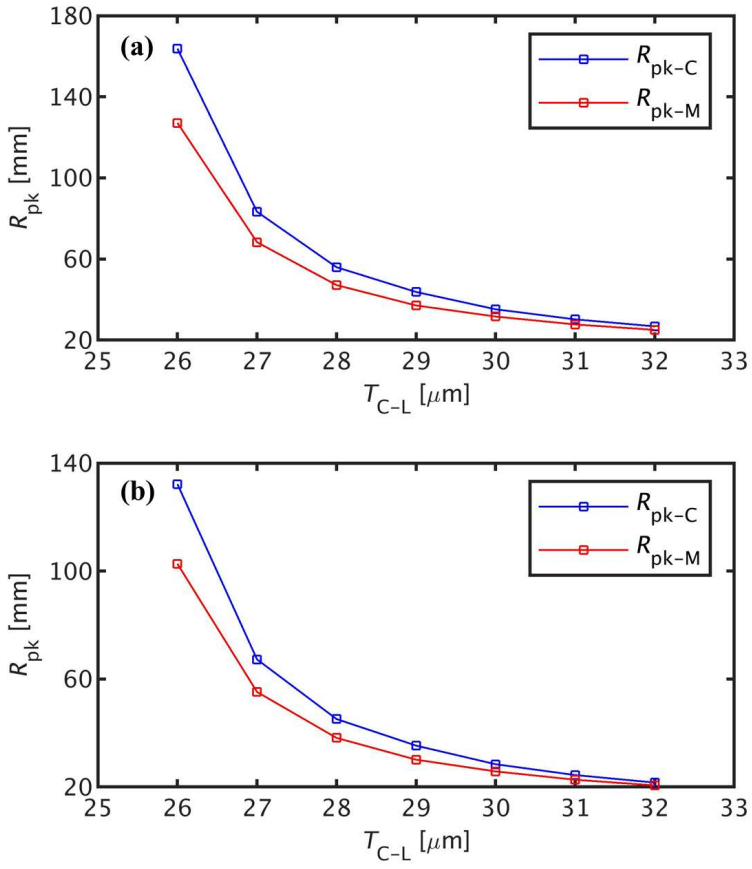

Fig. 20. Calculated R_{pk}s as functions of $T_{C\text{-}L}$ for O-band use: (a) $N_c = 8$; (b) $N_c = 10$.

Figures 20 (a) and (b) plot the $R_{pk\text{-}C}$ and $R_{pk\text{-}M}$ as functions of $T_{C\text{-}L}$ for N_c = 8 and 10, respectively. When $T_{C\text{-}L}$ equals to 25 μm, we use core A (the magenta dot in Fig. 11) to design Homo-SI-MCFs, so there are no critical bending radii plotted in Figs. 20 (a) and (b). When $T_{C\text{-}L}$ reaches 26 μm, R_{pk} of the designed Hetero-MCFs are calculated by Eq. (22). It is also clear that $R_{pk\text{-}M} < R_{pk\text{-}C}$ in all the cases, which indicates that the proposed method enables us to improve the R_{pk} of Hetero-SI-MCFs.

Improvement in XTs

Here, we also plot the XT values calculated using the analytical expression derived in Section 2. 1 and those calculated using FEM simulations, to show the good accuracy of the derived expression for estimating the XT in Hetero-SI-MCFs.

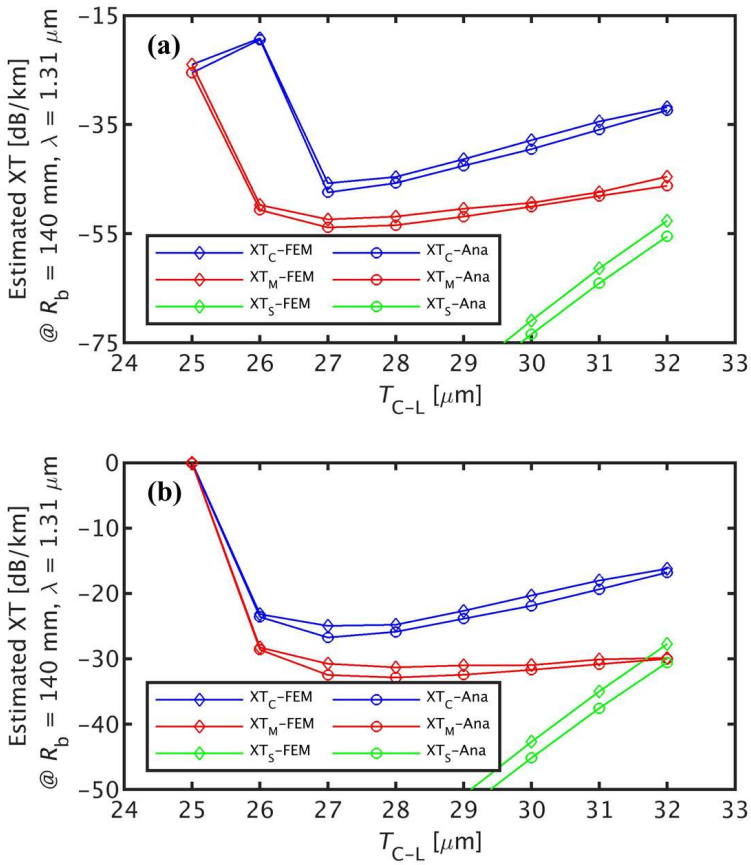

Fig. 21. Calculated XTs as functions of $T_{C\text{-}L}$ for O-band: (a) N_c = 8; (b) N_c = 10.

Figures 21 (a) and (b) plot the XT_C, XT_M, and XT_S as functions of $T_{C\text{-}L}$, where XTs are calculated at R_b = 140 mm and λ = 1310 nm, and d is assumed to be 1 m. When T_C = 25 μm, the XT of the Homo-

SI-MCFs designed using the core A represented by the magenta dot marked in Fig. 11 (a) is plotted, so $XT_C = XT_M$. When $T_C > 25$ μm, the XT_C of the conventional Hetero-SI-MCFs designed using the core combinations represented by dots of the same color depicted in Fig. 11 (a) and (b) is plotted, whereas the XT_M of the modified Hetero-SI-MCFs designed using the core A in Fig. 11 (a) and the core at the lower limit of *ECR* for different values of $T_{C\text{-}L}$ is plotted.

As shown in Fig. 21 (a), for $N_c = 8$, when $T_{C\text{-}L}$ equals to 26 μm, because the R_{pk} of conventional Hetero-MCF is larger than 140 mm, the XT_C is a relatively large value of the *R*-dominant region, whereas the R_{pk} of modified Hetero-MCF is smaller than 140 mm, so XT_M deceases into an ultra-low value of the *d*-dominant region. This indicates that the proposed method enables us to improve the R_{pk} of Hetero-SI-MCFs, and a large enough Δn_{eff} is necessary to ensure R_{pk} to be smaller than a certain value. When $T_{C\text{-}L}$ reaches 27 μm, the R_{pk}s of Hetero-MCFs are smaller than 140 mm, both the XT_C and XT_M decease into ultra-low values of the *d*-dominant region.

In the conventional Hetero-SI-MCFs, XT_C increases as $T_{C\text{-}L}$ increases, while in the modified Hetero-SI-MCFs, XT_M shows the best value at $T_{C\text{-}L} = 27$ μm, thereafter, it increases as $T_{C\text{-}L}$ increases. Here, we consider that K_{mn} is the dominant parameter for the conventional Hetero-SI-MCFs, resulting the increase of XT_C, while in the modified Hetero-SI-MCFs, the region of $T_{C\text{-}L} < 27$ μm is $\Delta\beta_{mn}$-dominant, which leads to the decrease of XT_M, and the region of $T_{C\text{-}L} > 27$ μm is K_{mn}-dominant, resulting the increase of XT_M. Accordingly, we propose the modified eight-core fiber with $T_{C\text{-}L} = 27$ μm from the perspective of the best XT_M value of −52.4 dB/km, which yields a total XT value of −49.4 dB/km and can be expected to support the transmission of QPSK format signals with a XT penalty of 1 dB over 1000 km [4].

The XT_S increases rapidly as $T_{C\text{-}L}$ increases, because it is smaller than −75 dB/km for $T_{C\text{-}L} < 30$ μm, that part of the green line is removed from Fig. 21 (a).

For $N_c = 10$, in the conventional Hetero-SI-MCFs, XT_C shows the best value at $T_{C\text{-}L} = 27$ μm, thereafter, the XT_C increases as $T_{C\text{-}L}$ increases, while in the modified Hetero-SI-MCFs, XT_M shows the best value at $T_{C\text{-}L} = 28$ μm, thereafter, the XT_M increases as $T_{C\text{-}L}$ increases. We consider that for the conventional Hetero-SI-MCFs, the region of $T_{C\text{-}L} < 27$ μm is $\Delta\beta_{mn}$-dominant, leading to the decrease of XT_C, and the region of $T_{C\text{-}L} > 27$ μm is K_{mn}-dominant, resulting the increase of XT_C. While for the modified Hetero-SI-MCFs, the region of $T_{C\text{-}L} < 28$ μm is $\Delta\beta_{mn}$-dominant, leading to the decrease of XT_M, and the region of $T_{C\text{-}L} > 28$ μm is K_{mn}-dominant, resulting the increase of XT_M. Accordingly, we propose the modified ten-core fiber with $T_{C\text{-}L} = 28$ μm from the perspective of the best XT_M value of

−31.3 dB/km, which yields a total XT value of −28.3 dB/km and can be expected to support the transmission of QPSK format signals with a XT penalty of 1 dB over 16 km [4].

The XT_S increases rapidly as $T_{C\text{-}L}$ increases and exceeds XT_M at $T_{C\text{-}L}$ = 32 μm, here, because XT_s is smaller than -50 dB/km for $T_{C\text{-}L}$ < 30 μm, that part of the green line is removed from Fig. 19 (b).

From Figs. 21 (a) and (b), it is also clear that $XT_M < XT_C$ in all the cases, which indicates that the proposed method enables us to improve the XT of Hetero-SI-MCFs.

3.2.3. *Fabrication errors in core parameter*

It is pointed out that in the uncoupled MCFs with fabrication errors, random structural fluctuation plays an important rule to determine the XT, and the fabrication error should be considered when design the uncoupled MCFs [34].

Therefore, in this section, by assuming the certain fabrication errors in core parameters, the errors in the values of R_{pk} and XT of the designed Hetero-SI-MCFs are discussed.

C-band

In the case of C-band, for the core A which is used for designing Homo-SI-MCFs, we consider that the fabrication error in the core radius is ± 0.01 μm, and the error in core Δ is ± 0.02%, namely, two more core as shown by the magenta circles on the A_{eff} = 80 μm^2 line in Fig. 22 (a) are used for discussion. For the cores at the upper limit and lower limit of *ECR*, we use one more core whose core radius is 0.01 μm smaller than that of the upper limit core and core Δ is 0.02% lower than that the upper limit core, and another one core whose core radius is 0.01 μm larger than that of the lower limit core and core Δ is 0.02% higher than that of the lower limit core to discuss the errors, these cores still have a A_{eff} of 80 μm^2 and are represented by circles with the same color as cores at the limits.

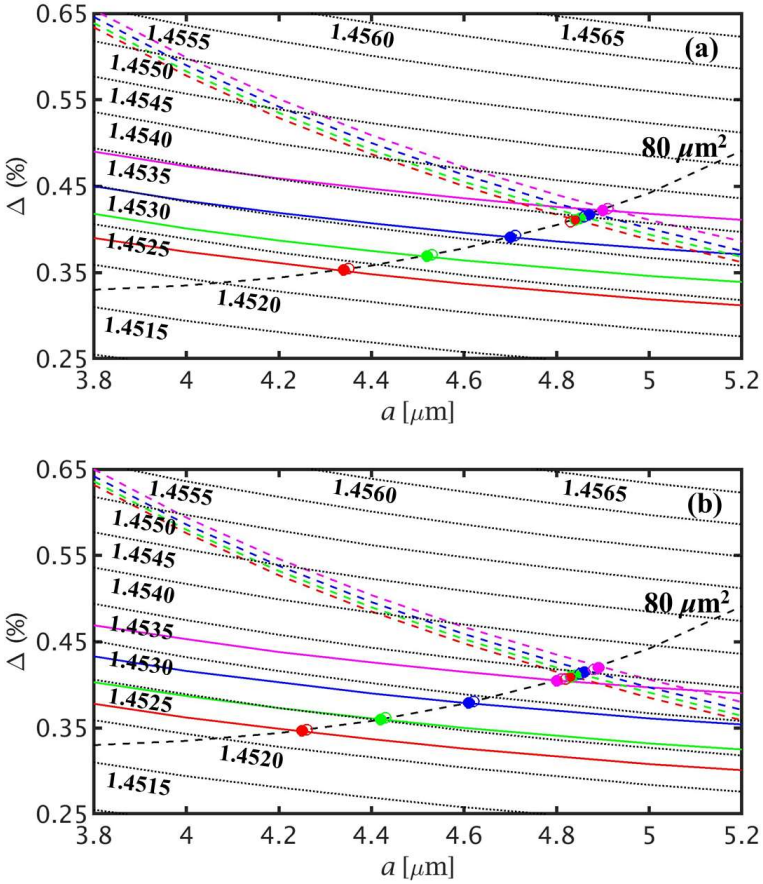

(a)	Cutoff limit	*EL* limit	(b)
T_C = 30 μm			T_C = 31 μm
T_C = 32 μm			T_C = 33 μm
T_C = 34 μm			T_C = 35 μm
T_C = 36 μm			T_C = 37 μm

Fig. 22. Relationship between the core parameters and effective indices for the C-band with the considerations of errors in core parameters: (a) T_C = 30, 32, 34, and 36 μm; (b) T_C = 31, 33, 35, and 37 μm.

Figures 23 (a) and (b) plot the $R_{pk\text{-}C}$ and $R_{pk\text{-}M}$ with the assumed errors in core parameters as functions of $T_{C\text{-}L}$ for N_c = 6 and 8, respectively. As shown by the positive error bars, it is easy to understand that the R_{pk} increases when two cores are not at the upper limit and lower limit, this is because the Δn_{eff} between two cores decreases when they are not at the upper limit and lower limit.

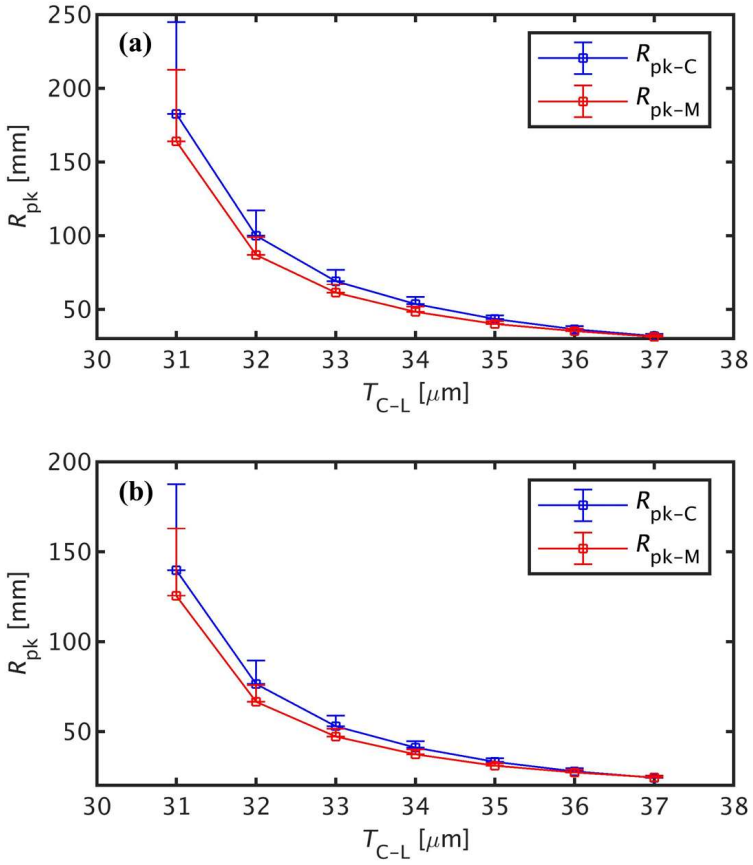

Fig. 23. Calculated R_{pk}s with the consideration of fabrication errors in core parameters as functions of $T_{C\text{-}L}$ for C-band: (a) $N_c = 6$; (b) $N_c = 8$.

Figures 24 (a) and (b) plot the XT_C, XT_M, and XT_S with the assumed errors in core parameters as functions of $T_{C\text{-}L}$, where XTs are still calculated at R_b = 140 mm and λ = 1550 nm, and d is assumed to be 1 m. Here, all the XT values are calculated using the FEM simulations, the colored circles represent XT values between the two cores at the upper limit and lower limit, and error bars indicate the errors in XT values due to the assumed fabrication errors. We can find that XT value between the two cores at the upper limit and lower limit is not always the lowest one because it is dependent on the K_{pq} as well as $\Delta\beta_{pq}$.

For six-core fibers, the error in XT_C with the assumed core parameter deviations is lower than 2.7 dB/km in all the cases, while the error in XT_M is lower than 2.5 dB/km. For eight-core fibers, the error in XT_C is lower than 2.3 dB/km in all the cases, while the error in XT_M is lower than 2.4 dB/km.

In the case of eight-core fibers, the positive error bars of XT_C and XT_M reach 0 dB/km at $T_{C\text{-}L}$ = 31 μm, this is because the R_{pk} surpass 140 mm when two cores are not at the upper limit and lower limit, resulting a large XT value of R-dominant region. This also indicates that a large enough Δn_{eff} is

required for Hetero-MCFs design.

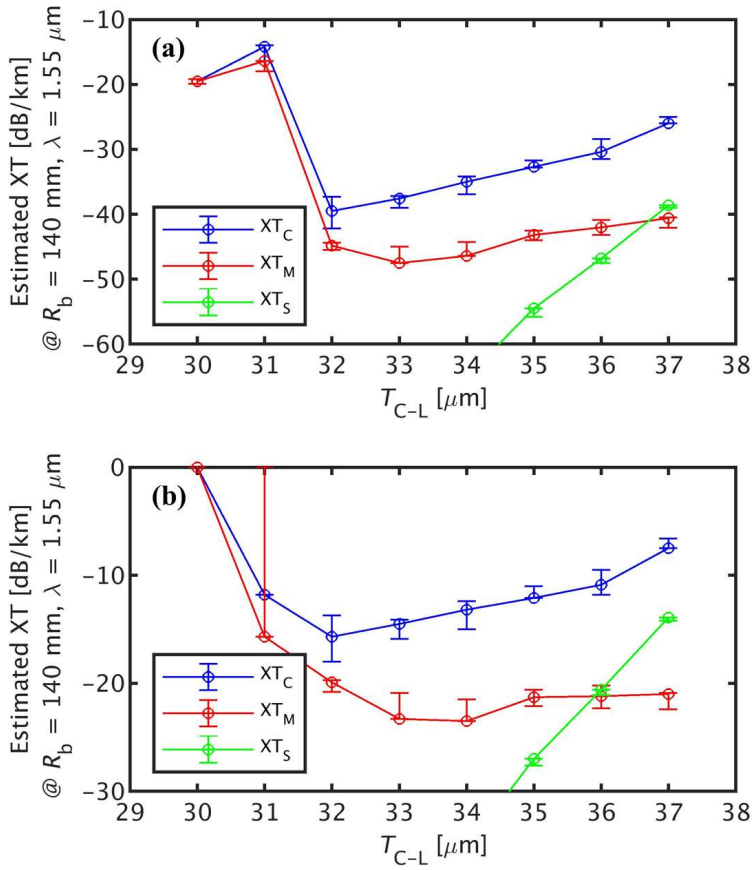

Fig. 24. Calculated XTs with the consideration of fabrication errors in core parameters as functions of $T_{C\text{-}L}$ for C-band use: (a) N_c = 6; (b) N_c = 8.

O-band

In the case of O-band, for the core A which is used for designing Homo-SI-MCFs, we consider that the fabrication error in the core radius is ± 0.02 μm, and the error in core Δ is ± 0.02%, namely, two more core as shown by the magenta circles on the A_{eff} = 55 μm^2 line in Fig. 25 (a) are used for discussion. For the cores at the upper limit and lower limit of *ECR*, we use one more core whose core radius is 0.02 μm smaller than that of the upper limit core and core Δ is 0.02% lower than that the upper limit core, and another one core whose core radius is 0.02 μm larger than that of the lower limit core and core Δ is 0.02% higher than that of the lower limit core to discuss the errors, these cores still have a A_{eff} of 55 μm^2 and are represented by circles with the same color as cores at the limits.

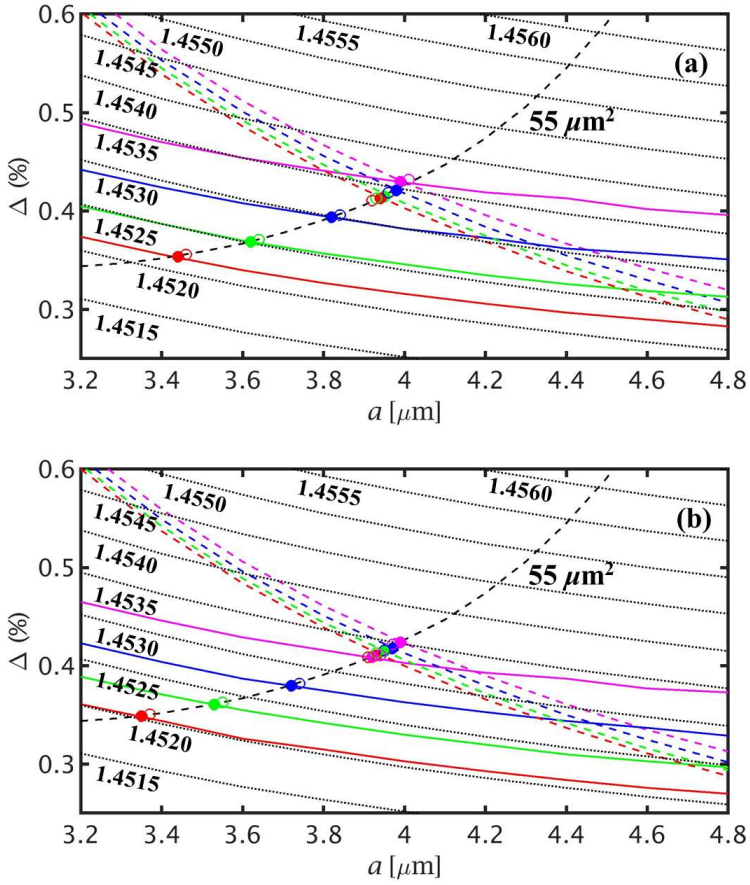

(a)	Cutoff limit	*EL* limit	(b)
T_C = 25 μm			T_C = 26 μm
T_C = 27 μm			T_C = 28 μm
T_C = 29 μm			T_C = 30 μm
T_C = 31 μm			T_C = 32 μm

Fig. 25. Relationship between the core parameters and effective indices for the O-band with the considerations of errors in core parameters: (a) T_C = 25, 27, 29, and 31 μm; (b) T_C = 26, 28, 30, and 32 μm.

Figures 26 (a) and (b) plot the $R_{pk\text{-}C}$ and $R_{pk\text{-}M}$ with the assumed errors in core parameters as functions of $T_{C\text{-}L}$ for N_c = 8 and 10, respectively. As shown by the positive error bars, we can see that the R_{pk} increases when two cores are not at the upper limit and lower limit, which can be attributed to the fact of the reduction of Δn_{eff}.

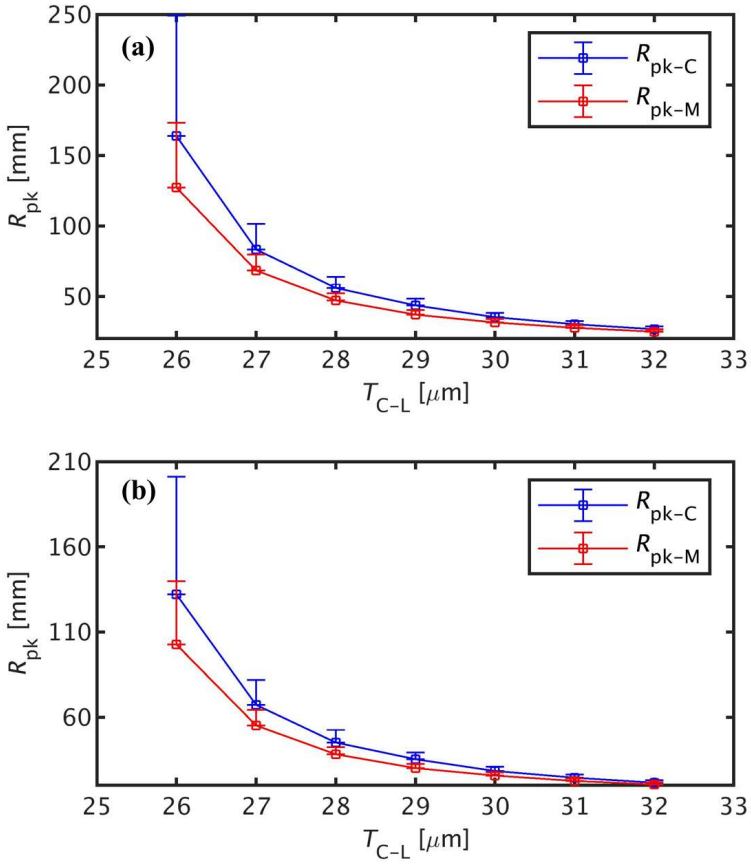

Fig. 26. Calculated R_{pk}s with the consideration of fabrication errors in core parameters as functions of $T_{C\text{-}L}$ for O-band: (a) N_c = 8; (b) N_c = 10.

Figures 27 (a) and (b) plot the XT_C, XT_M, and XT_S with the assumed errors in core parameters as functions of $T_{C\text{-}L}$, where XTs are calculated at R_b = 140 mm and λ = 1310 nm, and d is assumed to be 1 m.

For eight-core fibers, the error in XT_C with the assumed core parameter deviations is lower than 2.7 dB/km in all the cases, while the error in XT_M is lower than 2.1 dB/km. For ten-core fibers, the error in XT_C is lower than 2.2 dB/km in all the cases, while the error in XT_M is lower than 1.9 dB/km.

In the case of eight-core fibers, the positive error bars of XT_M reach around XT_C at $T_{C\text{-}L}$ = 26 μm, this is because the R_{pk} surpass 140 mm when two cores are not at the upper limit and lower limit, resulting a large XT value of R-dominant region.

In the case of ten-core fibers, the positive error bars of XT_C and XT_M reach 0 dB/km at $T_{C\text{-}L}$ = 26 μm, this is because the R_{pk} surpass 140 mm when two cores are not at the upper limit and lower limit, resulting a large XT value of R-dominant region, which also indicates that a large enough Δn_{eff} is required for Hetero-MCFs design.

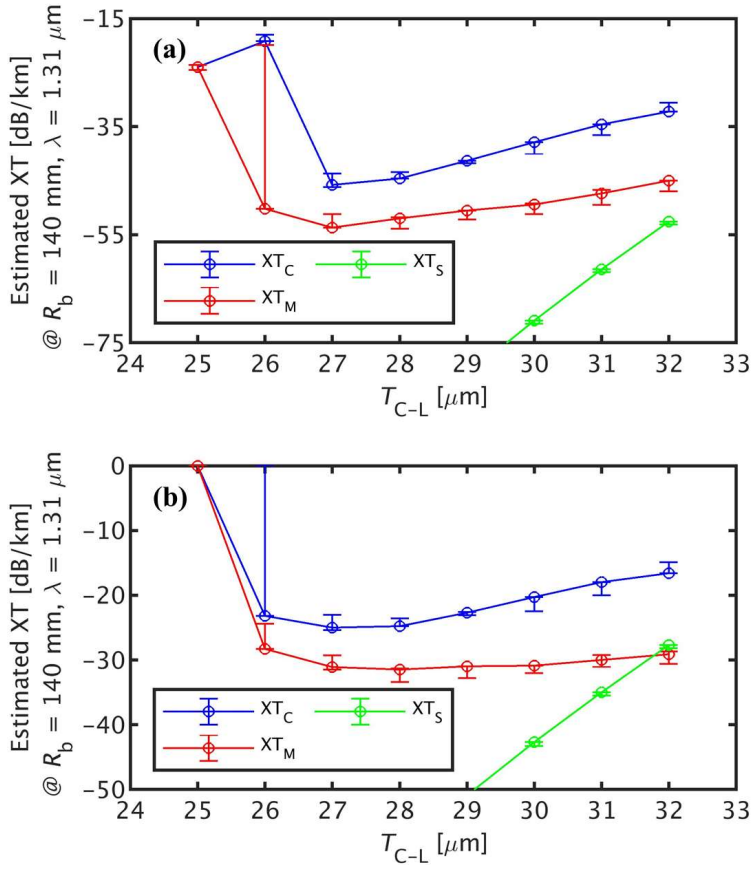

Fig. 27. Calculated XTs with the consideration of fabrication errors in core parameters as functions of $T_{C\text{-}L}$ for O-band: (a) N_c = 8; (b) N_c = 10.

3.3 Conclusion

Using the proposed method of the core allocation in Hetero-MCFs, we achieved six-core fibers with small R_{pk} and sufficient low XT within 125-μm standard cladding diameter by the simple SI profile. It has been shown that the standard cladding diameter supports eight simple SI non-identical cores with acceptable XT for C-band.

For O-band use, the number of cores that can be incorporated in the standard cladding diameter is same as that of the conventional Hetero-SI-MCFs. However, it has been shown that the XT values have a suppression of approximately 8 dB/km in all the cases as compared to the conventional cases. The designed Hetero-SI-MCFs are shown in the following sections.

Designed modified Hetero-SI-MCFs for C-band

The cross sections of the designed modified six-core and eight-core Hetero-SI-MCFs for C-band are shown in Fig. 28 (a) and (b), respectively. In both cases, cores with higher core refractive index are allocated to the circle with $T_{C\text{-}H}$ = 30 μm, cores with lower core refractive index are allocated to the circle with $T_{C\text{-}L}$ = 33 μm in the six-core fiber, while cores with lower core refractive index are allocated to the circle with $T_{C\text{-}L}$ = 34 μm in the eight-core fiber.

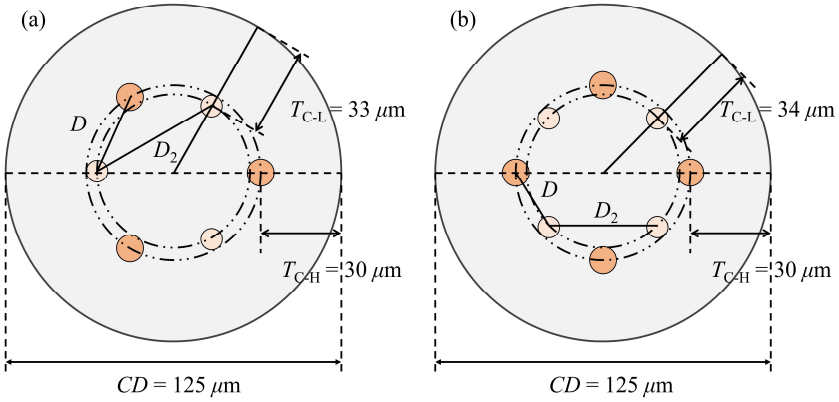

Fig. 28. Cross sections of the designed modified Hetero-SI-MCFs for C-band. (a) 6-core fiber. (b) 8-core fiber.

The core parameters used for the designed modified Hetero-SI-MCFs for C-band are listed in Table V, where core A is the one with higher core refractive index marked by magenta dot in Fig. 8 (a). Core S_L is the one with lower core refractive index in the six-core fiber, while core E_L is the one with lower core refractive index in the eight-core fiber. The main parameters of the designed modified Hetero-SI-MCFs for C-band are listed in Table VI.

Table. V Core parameters of the designed modified Hetero-SI-MCFs for C-band.

Core number	a [μm]	Δ [%]	A_{eff} [μm^2]
A	4.90	0.422	80.1
S_L	4.61	0.379	80.1
E_L	4.52	0.369	80.1

Table. VI Parameters of the designed modified Hetero-SI-MCFs for C-band.

N_c	D [μm]	D_2 [μm]	R_{pk} [mm]	XT [dB/km]
6	31.1	51.1	61.3	−44.5
8	23.6	40.3	37.2	−20.4

Figures 29 (a) and (b) plot the calculated nearest XT between the adjacent non-idnetical cores as functions of R_b for the designed six- and eight-core fibers, respectively. XT is calculated at λ = 1550 nm, and d is assumed to be 1 m, 10 m, and 100 m, respectively. In both MCFs, the XT increases as R_b increases in the R-dominant region, whereas the XT decreases into an ultra-low value and remains insensitive to R_b in the d-dominant region. In Fig. 29 (b), the XT value of the designed eight-core fiber recheas 0 db/km at the R-dominant region.

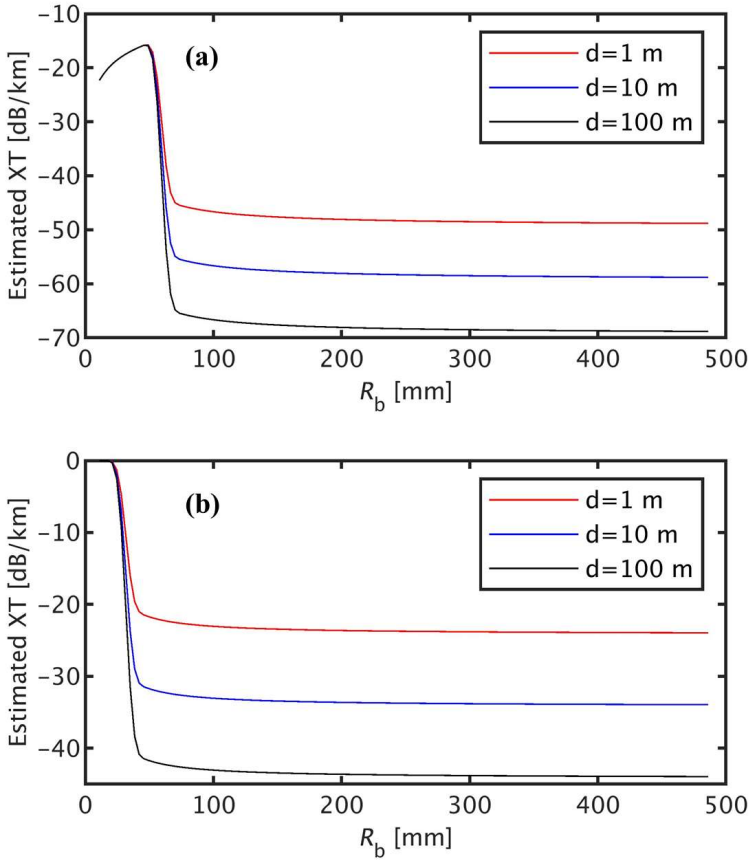

Fig. 29. Nearest XT between the adjacent cores in the designed modified Hetero-SI-MCFs for C-band. (a) 6-core fiber. (b) 8-core fiber.

Designed modified Hetero-SI-MCFs for O-band

The cross sections of the designed modified eight-core and ten-core Hetero-SI-MCFs for O-band are

shown in Fig. 30 (a) and (b) respectively. In both cases, cores with higher core refractive index are allocated to the circle with $T_{C\text{-}H}$ = 25 μm, cores with lower core refractive index are allocated to the circle with $T_{C\text{-}L}$ = 27 μm in the six-core fiber, while cores with lower core refractive index are allocated to the circle with $T_{C\text{-}L}$ = 28 μm in the eight-core fiber.

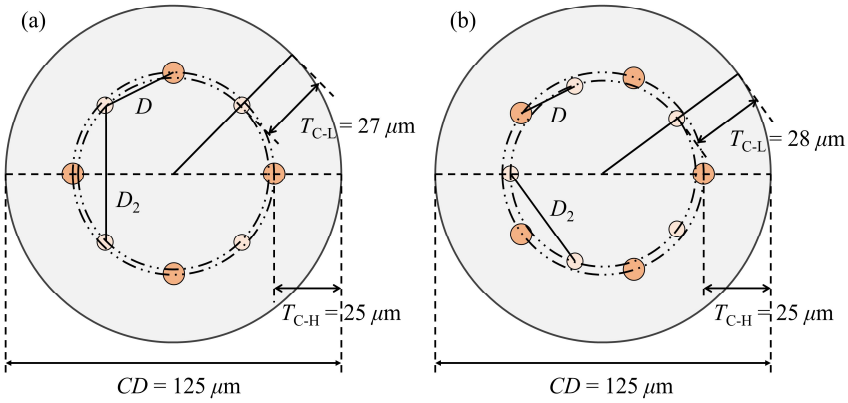

Fig. 30. Cross sections of the designed modified Hetero-SI-MCFs for O-band. (a) 8-core fiber. (b) 10-core fiber.

The core parameters used for the designed modified Hetero-SI-MCFs for O-band are listed in Table VII, where core A is the one with higher core refractive index marked by magenta dot in Fig. 11 (a). Core E_L is the one with lower core refractive index in the eight-core fiber, while core T_L is the one with lower core refractive index in the ten-core fiber. The main parameters of the designed modified Hetero-SI-MCFs for O-band are listed in Table VIII.

Table. VII Core parameters of the designed modified Hetero-SI-MCFs for O-band.

Core number	a [μm]	Δ [%]	A_{eff} [μm^2]
A	3.99	0.430	54.6
E_L	3.82	0.394	55.0
T_L	3.72	0.380	55.0

Table. VIII Parameters of the designed modified Hetero-SI-MCFs for O-band.

N_c	D [μm]	D_2 [μm]	R_{pk} [mm]	XT [dB/km]
8	28.0	50.2	68.3	−49.4

10	22.4	40.6	38.2	−28.3

Figures 31 (a) and (b) plot the calculated nearest XT between the adjacent non-idnetical cores as functions of R_b for the designed six- and eight-core fibers, respectively. XT is calculated at λ = 1310 nm, and d is assumed to be 1 m, 10 m, and 100 m, respectively. In both MCFs, the XT increases as R_b increases in the R-dominant region, whereas the XT decreases into an ultra-low value and remains insensitive to R_b in the d-dominant region.

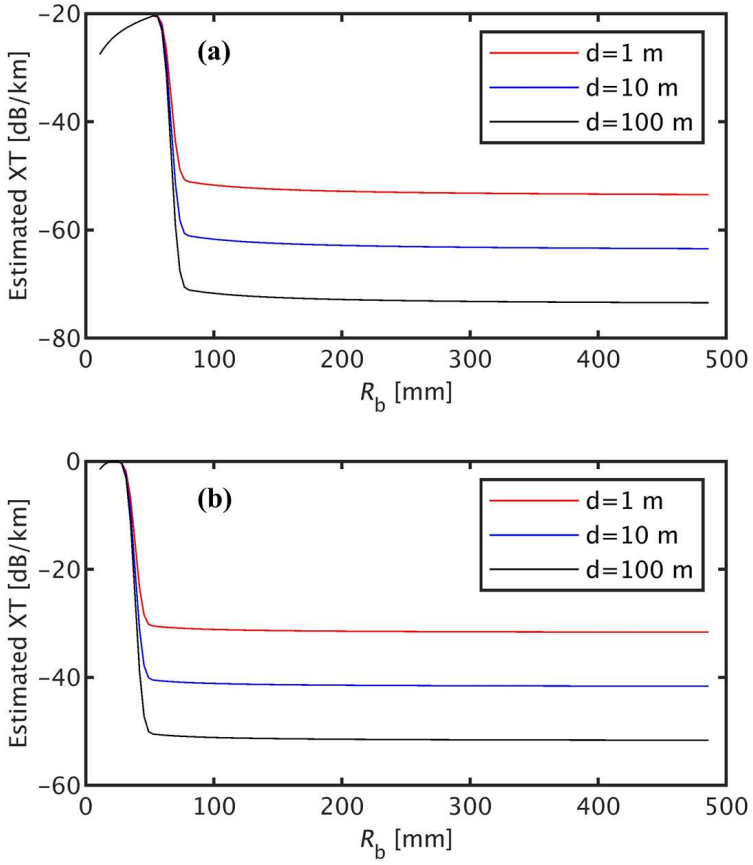

Fig. 31. Nearest XT between the adjacent cores in the designed modified Hetero-SI-MCFs for O-band. (a) 8-core fiber. (b) 10-core fiber.

4 *Chapter 4. The outer trench layer*

4.1 Schematic of the outer trench layer

A low refractive index outer trench (OT) layer is proposed to suppress the confinement loss (*CL*) of cores in MCFs. Fig. 32 shows the schematic of the proposed MCFs, OT layer is the gray region of the outermost part of the standard cladding with a relatively low refractive index. W_{OT} and Δ_{OT} stands for the thickness of OT layer and the relative refractive index difference between OT layer and standard cladding, respectively. T_C is the outer cladding thickness. *D* represents the core pitch, and *CD* represents the cladding diameter which is also fixed as 125-μm..

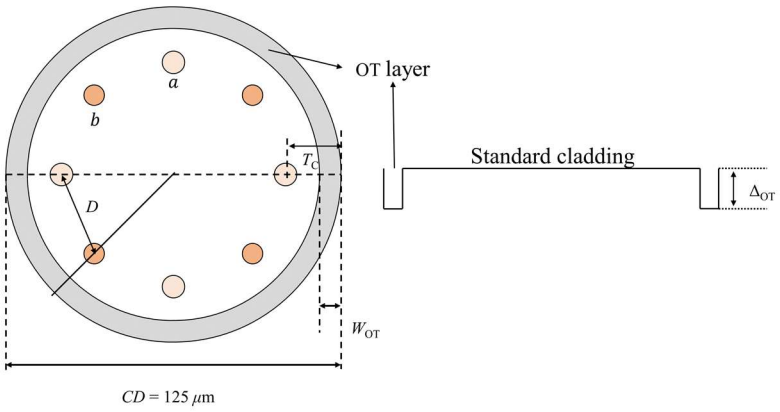

Fig. 32. Schematic of the proposed outer trench layer for MCFs.

4.2 Applications of the outer trench layer

In this section, the steps of designing MCFs with OT layer are presented. Firstly, we select two cores *a* and *b* with $\Delta n_{eff} = 0.00063$ [2], which can be expected to realize the lowest XT for non-identical cores. Then to meet a certain value of XT, we determine the core pitch between these two cores. Lastly, we discuss how the loss of cores changes with W_{OT}, and determine the preferable structure of OT layer.

Selections of core parameter

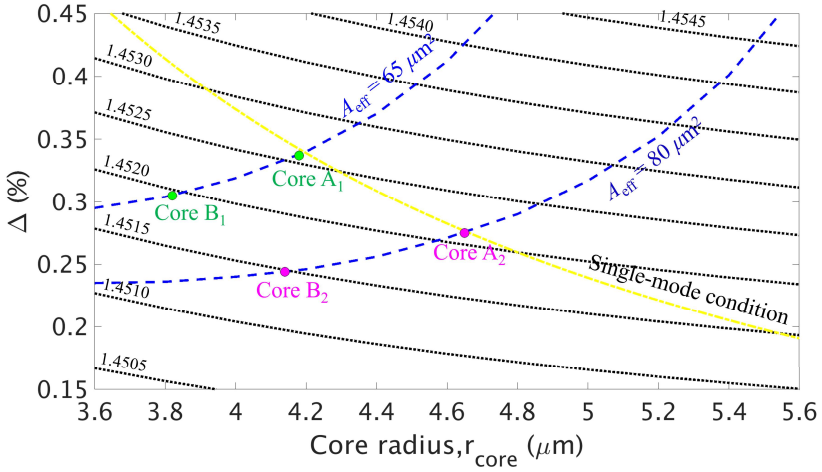

Fig. 33. Relationship between the core parameters and effective indices

As mentioned before, cores with different n_{eff} will produce different A_{eff}, which is required to be same for realizing homogeneity of transmission characteristics. Fig. 33 shows the method to select the parameters of non-identical cores.

Here, A_{eff} of 80 μm^2 is the general recommendation for SSMF, based on the consideration of XT and *CL*, for short-link transmission, the A_{eff} can be sacrificed into 65 μm^2 which is a comparable value to those of the cores in paper [10].

In [2], both the calculated results and measured XT values presented that the correlation length *d* which is the single parameter to estimate the XT value between heterogeneous cores should be more than 1 m. Furthermore, when cores with a Δn_{eff} of 0.00063, the XT showed best value which can be estimated by correlation length *d* of 100 m. Based on these, in this kind of fiber design, we focus on choosing cores with $\Delta\Delta n_{\mathrm{eff}} = 0.00063$. Core combinations with with $A_{\mathrm{eff}} = 65$ μm^2 and $A_{\mathrm{eff}} = 80$ μm^2 are selected in Fig. 33, and the core parameters are listed out in the following Table.

Table. IX Core parameters of the designed Hetero-SI-MCFs with OT

Core number	a [μm]	Δ [%]	A_{eff} [μm^2]
A_1	4.18	0.337	65.1
B_1	3.82	0.415	65.1
A_2	4.65	0.275	80.1
B_2	4.14	0.244	80.1

Then, we can calculate the XT, R_{pk}, and loss of these cores. Here, the target value of XT is assumed to be lower than −40 dB after 10 km transmission [10].

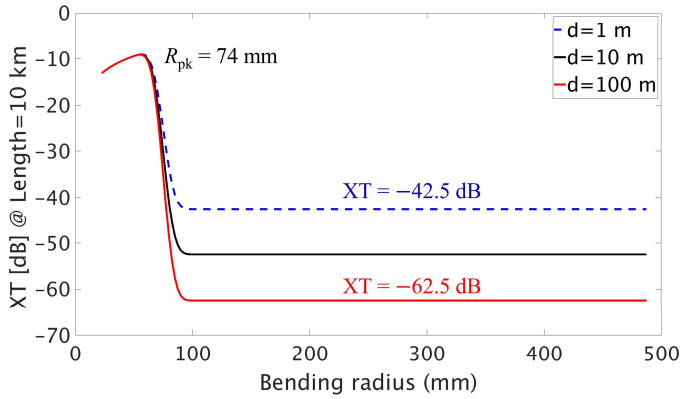

Fig. 34. Calculated 10 km XT at 1.31 μm for core combination with A_{eff} = 65 μm^2.

Figure 34 plots the 10 km XT between the two cores with A_{eff} = 65 μm^2 for the core pitch is 32 μm. Here, we focus on the XT value estimated by d = 1 m, because it is a more general value for non-identical cores. it is found that the core pitch needs to be large than 32 μm to make their XT value to be lower than −40 dB. therefore, we determined that the core pitch is 32 μm for these two cores. Here, we should note that these core combinations can be expected to get a XT value estimated by d = 100 m, which is significantly lower than that by d = 1 m as shown in Fig. 34.

Parameters of the OT layer

We then research how the loss of cores change with the parameters of OT layer.

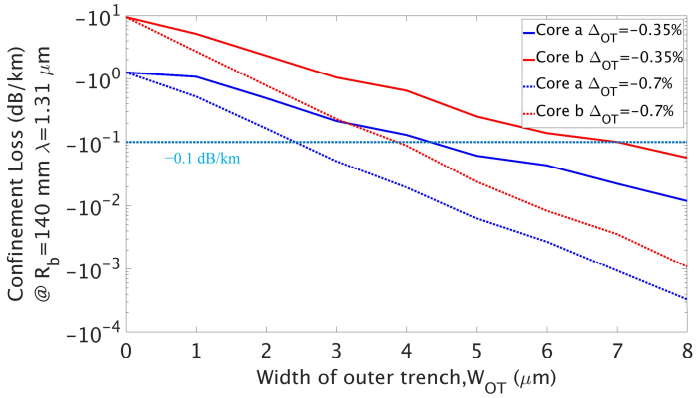

Fig. 35. Relationship between loss of cores and W_{OT} for core combination with A_{eff} = 65 μm^2.

Suppose we incorporate 8 cores in the standard cladding diameter, in the case of core pitch of 32 μm, T_C is shortened to be 20.7 μm now, which is relatively small than the minimum T_C of 25 μm that we used in the previous sections. Therefore, low-index trench layer is required to help us make the loss of core to meet a certain target value.

Fig. 35 shows the relationship between loss of cores and OT properties for core combination with A_{eff} of 65 μm^2. The loss is estimated at bending radius of 140 mm and λ = 1.31 μm. W_{OT} ranges from 0 to 8 μm, and Δ_{OT} is set as −0.35% and −0.7% respectively, which are the general values that used in the trench-assisted core design.

When W_{OT} is 0, the fiber structure is the same as those conventional MCFs just contain the core region and standard cladding region without OT layer, because the T_C of cores are too thin, the loss of cores is extremely large. We can see that the loss decreases as the W_{OT} increases. In addition to this, deep trench (Δ_{OT} = −0.7%) has better suppression in the loss as compared with the shallow trench (Δ_{OT} = −0.35%). Therefore, we can either change W_{OT} or Δ_{OT} to achieve the target loss limit of −0.1 dB/km.

In Fig. 35, we can find that OT properties of W_{OT} = 8 μm with Δ_{OT} = −0.35% and W_{OT} = 5 μm with Δ_{OT} = −0.7% both achieved the target loss limit of −0.1 dB/km. However, deeper trench structures generally increase the cost of fabrication process since a large amount of fluorine dopant is required [12]. We prefer the OT structure of W_{OT} = 8 μm with Δ_{OT} = −0.35% in the proposed fiber structure.

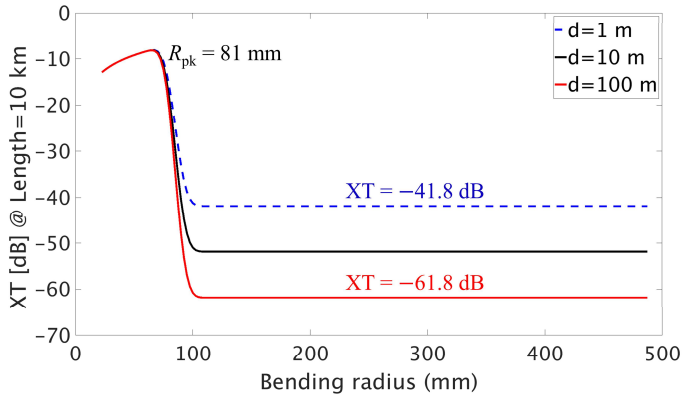

Fig. 36. Calculated 10 km XT at 1.31 μm for core combination with A_{eff} = 80 μm^2.

Same as previous part, figure 36 plots the 10 km XT between the two cores with A_{eff} = 80 μm^2 for the core pitch of 35 μm. Here we also focus on the XT value estimated by d = 1 m, because it is a more general value for non-identical cores. It is found that the core pitch needs to be large than 35 μm to

make their XT value to be lower than −40 dB. Therefore, we determined that the core pitch is 35 μm for these two cores. Here, we should note that these core combinations can be expected to get a XT value estimated by d = 100 m, which is significantly lower than that by d = 1 m as shown in Fig. 36.

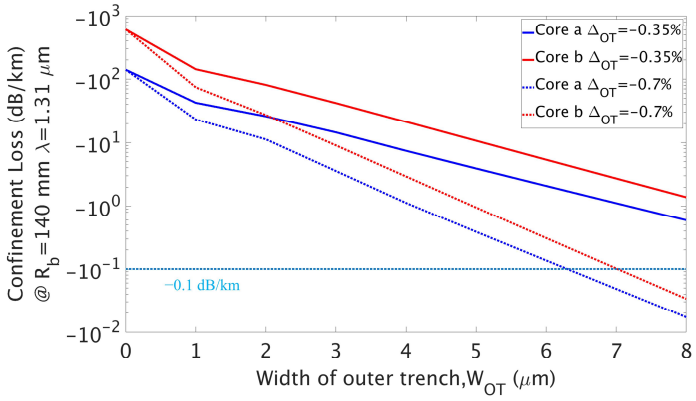

Fig. 37. Relationship between loss of cores and W_{OT} for core combination with A_{eff} = 80 μm^2.

Suppose we also attempt to incorporate 8 cores in the standard cladding diameter, in the case of core pitch is 35 μm, T_C is further shortened to be 16.8 μm now, so the low-index trench layer is required to help us make the loss of core to meet a certain target value.

Fig. 37 shows the relationship between loss of cores and OT properties for core combination with A_{eff} of 80 μm^2. The loss is also estimated at bending radius of 140 mm and λ = 1.31 μm. W_{OT} ranges from 0 to 8 μm, and Δ_{OT} is set as −0.35% and −0.7% respectively.

We can see that the loss decreases as the W_{OT} increases, and also, the deep trench (Δ_{OT} = −0.7%) has better suppression in the loss as compared with the shallow trench (Δ_{OT} = −0.35%). We can either change W_{OT} or Δ_{OT} to achieve the target loss limit of −0.1 dB/km.

In Fig. 37, we can find that OT properties with Δ_{OT} = −0.35% is no longer enough to achieve the target loss limit of −0.1 dB/km, the OT structure with Δ_{OT} = −0.7% and W_{OT} = 8 μm is required in the proposed fiber structure.

4.3 Conclusion

Using the proposed low refractive index OT layer, it has been shown that the outer cladding thickness of MCFs can be shortened to a smaller value, which allows us to enlarge the core pitch of cores. MCFs

with OT layer structures also enables us to achieve 8-core fibers sufficient low XT within 125-μm standard cladding diameter by the simple SI profile.

Designed Hetero-SI-MCFs with OT

The cross sections of the designed eight-core Hetero-SI-MCFs with OT layer with different effective core area are shown in Fig. 38 (a) and (b) respectively. In the case of $A_{\mathrm{eff}} = 65\ \mu\mathrm{m}^2$, cores are allocated to the circle with $T_{\mathrm{C}} = 32\ \mu$m with one-ring core layout, the fiber has an OT layer of $W_{\mathrm{OT}} = 8\ \mu$m with $\Delta_{\mathrm{OT}} = -0.35\%$, whereas in the case of $A_{\mathrm{eff}} = 80\ \mu\mathrm{m}^2$, cores are allocated to the circle with $T_{\mathrm{C}} = 35\ \mu$m with one-ring core layout, the fiber has an OT layer of $W_{\mathrm{OT}} = 8\ \mu$m with $\Delta_{\mathrm{OT}} = -0.7\%$

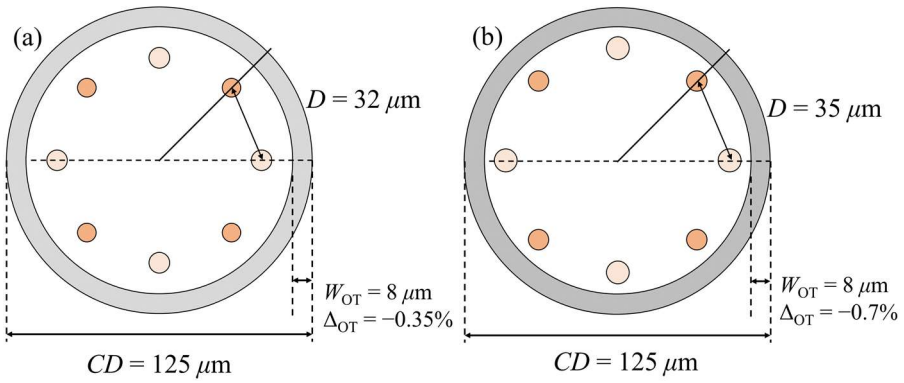

Fig. 38. Cross sections of the designed Hetero-SI-MCFs with OT. (a) $A_{\mathrm{eff}} = 65\ \mu\mathrm{m}^2$. (b) $A_{\mathrm{eff}} = 65\ \mu\mathrm{m}^2$.

The main parameters of the designed Hetero-SI-MCFs with OT layer are listed in Table X.

Table. X Parameters of the designed Hetero-SI-MCFs with OT

N_{c}	W_{OT} [μm]	T_{C} [μm]	R_{pk} [mm]	XT [dB/10 km]
8	8	20.7	74	−42.5
8	8	16.8	81	−41.8

5 *Chapter 5. Summary*

An analytical expression for the mode-coupling coefficient between non-identical SI cores is derived, which enables a quick estimation of the XT values in Hetero-SI-MCFs. The derived analytical expression has a good accuracy as compared with the most rigorous numerical simulations by FEM, it has been shown that the error in XT values obtained using the derived expression and those obtained using FEM simulations is lower than −2 dB/km.

Using the derived expression, the feasibility of Hetero-SI-MCF design within the standard 125-μm is discussed. It has been shown that the simple SI profile enables us to allocate four and six non-identical cores in the 125-μm cladding diameter for the long-haul and short-reach transmissions of C-band, respectively, and the number of cores can be increased to eight and ten for the long-haul and short-reach transmissions of O-band, respectively.

A novel core allocation for the Hetero-MCFs is proposed, which enables us to improve the critical bending radius (R_{pk}) and XT values of fibers. With this method, it has been shown that the simple SI profile enables us to allocate six and eight non-identical cores in the 125-μm cladding diameter for the long-haul and short-reach transmissions of C-band, respectively. In comparison with the conventional Hetero-SI-MCFs with one-ring core layout, the number of cores is increased by 2. For the O-band, we are still limited to allocate eight and ten for the long-haul and short-reach transmissions of O-band, respectively. However, all the R_{pk}s XT values are significantly improved. This proposed method can be also expected to improve XT and R_{pk} of Hetero-TA-MCFs.

An outer trench (OT) layer with relatively low refractive index is proposed, which enables us to suppress the loss of outer cores in the MCFs. With this method, it has also been shown that the simple SI profile enables us to allocate eight non-identical cores in the 125-μm cladding diameter with the sufficiently low XT for the O-band transmission.

Hetero-SI-MCF design that combined with the two proposed method of core allocation and OT layer can be expected to further improve the critical bending radius (R_{pk}) and XT values. However, the fabrication complexity and cost become other issues that need to be concerned.

References

[1] T. Morioka, “New generation optical infrastructure technologies: ‘EXAT Initiative’ Towards 2020 and Beyond,” *Proc. Opt. Electron. Commun. Conf. (OECC)*, Paper FT4, July 2009.

[2] Y. Amma, Y. Sasaki, K. Takenaga, S. Matsuo, J. Tu, K. Saitoh, M. Koshiba, T. Morioka, and Y. Miyamoto, “High-density multicore fiber with heterogeneous core arrangement,” *Proc. Opt. Fiber Commun. Conf. (OFC)*, Paper Th4C.4, Mar. 2015.

[3] Y. Sasaki, S. Saitoh, Y. Amma, K. Takenaga, S. Matsuo, K. Saitoh, T. Morioka, and Y. Miyamoto, “Quasi-single-mode homogeneous 31-core fiber,” *Proc. Eur. Conf. Exhib. Opt. Commun. (ECOC)*, Paper We.1.4.4, Sep. 2015.

[4] P. J. Winzer, A. H. Gnauck, A. Konczykowska, F. Jorge, and J. Y. Dupuy, “Penalties from in-band crosstalk for advanced optical modulation formats,” *Proc. Eur. Conf. Exhib. Opt. Commun. (ECOC)*, Paper Tu.5.B.7, Sep. 2011.

[5] K. Takenaga, Y. Sasaki, N. Guan, S. Matsuo, M. Kasahara, K. Saitoh, and M. Koshiba, “Large effective-area few-mode multicore fiber,” *Opt. Lett.*, vol. 24, no. 21, pp. 1941–1944, Nov. 1, 2012.

[6] J. Sakaguchi, W. Klaus, J.-M. D. Mendinueta, B. J. Puttnam, R. S. Luis, Y. Awaji, N. Wada, T. Hayashi, T. Nakanishi, T. Watanabe, Y. Kokubun, T. Takahata, and T. Kobayashi, “Realizing a 36-Core, 3-mode fiber with 108 spatial channels,” *Proc. Opt. Fiber Commun. Conf. (OFC)*, Paper Th5C.2, Mar. 2015.

[7] K. Igarashi, D. Souma, Y. Wakayama, K. Takeshima, Y. Kawaguchi, T. Tsuritani, I. Morita, and M. Suzuki, “114 space-division-multiplexed transmission over 9.8-km weakly-coupled-6-mode uncoupled-19-core fibers,” *Proc. Opt. Fiber Commun. Conf. (OFC)*, Paper Th5C.4, Mar. 2015.

[8] T. Matsui, Y. Yamada, Y. Sagae, and K. Nakajia, “Standard cladding diameter multi-core fiber technology,” *Proc. Opt. Fiber Commun. Conf. (OFC)*, Paper Tu6B.4, Jun. 2021.

[9] S. Matsuo, K. Takenaga, Y. Sasaki, Y. Amma, S. Saito, K. Saitoh, T. Matsui, K. Nakajima, T. Mizuno, H. Takara, Y. Miyamoto, and T. Morioka, “High-spatial-multiplicity multicore fibers for future dense space-division-multiplexing systems,” *J. Lightw. Technol.*, vol. 34, no. 6, pp. 1464–1475, Mar. 2016.

[10] T. Hayashi, T. Nakanishi, K. Hirashima, O. Shimakawa, F. Sato, K. Koyama, A. Furuya, Y. Murakami, and T. Sasaki, "125-μm-cladding eight-core multi-core fiber realizing ultra-high-density cable suitable for O-band short-reach optical interconnects," *J. Lightw. Technol.*, vol. 34, no.1, pp. 85–92, Jan. 2016.

[11] T. Matsui, Y. Sagae, T. Sakamoto, and K. Nakajima, "Design and applicability of multi-core fibers with standard cladding diameter," *J. Lightw. Technol.*, vol. 38, no. 21, pp. 6065–6070, Nov. 2020.

[12] Y. Sasaki, M. Ozeki, K. Takenaga, and K. Aikawa, "Asymmetrically arranged 8-core fibers with center core suitable for side-view alignment in datacenter networks," *Proc. Opt. Fiber Commun. Conf. (OFC)*, Paper T4J.1, Feb. 2020.

[13] T. Matsui, T. Sakamoto, Y. Goto, K. Saito, K. Nakajima, F. Yamamoto, and T. Kurashima, "Design of 125 μm cladding multi-core fiber with full-band compatibility to conventional single-mode fiber," *Proc. Eur. Conf. Exhib. Opt. Commun. (ECOC)*, Paper We.4.3, Sep. 2015.

[14] Y. Sagae, T. Matsui, T. Sakamoto, and K. Nakajima, "Ultra-Low crosstalk multi-core fiber with standard 125-μm cladding diameter for 10,000km-class long-haul transmission," *IEICE Trans. Commun.*, vol. E103-B, no 11, 1199-1205, Nov. 2020.

[15] M. Takahashi, K. Maeda, K. Aiso, K. Mukasa, R. Sugizaki, D. Soma, H. Takahashi, T. Tsuritani, M. Mitrovic, B. Pálsdóttir, and Y. Arashitani "Uncoupled 4-core fibre with ultra-low loss and low inter core crosstalk," *Proc. Eur. Conf. Exhib. Opt. Commun. (ECOC)*, Th1.A1-5. Dec. 2020.

[16] K. Takenaga, Y. Arakawa, Y. Sasaki, S. Tanigawa, S. Matsuo, K. Saitoh, and M. Koshiba, "A large effective area multi-core fiber with an optimized cladding thickness," *Opt. Exp.*, vol. 19, no. 26, pp. B543–B550, Dec. 2011.

[17] K. Takenaga, Y. Arakawa, S. Tanigawa, N. Guan, S. Matsuo, K. Saitoh, and M. Koshiba, "Reduction of crosstalk by trench-assisted multi-core fiber," *Proc. Opt. Fiber Commun. Conf. (OFC)*, Paper OWJ4, Mar. 2011.

[18] K. Saitoh, T. Matsui, T. Sakamoto, M. Koshiba, and S. Tomita, "Multi-core hole-assisted fibers for high core density space division multiplexing," *Proc. Opt. Electron. Commun. Conf. (OECC)*, Paper 7C2-1, July 2010.

[19] X. Xie, J. Tu, K. Long, and K. Saitoh, "Heterogeneous 32-core fiber with square-lattice layout for high-density transmissions," *Proc. Asia Commun. Photon. Conf. (ACP)*, Paper AS2A, Nov. 2016.

[20] M. Koshiba, K. Saitoh, and Y. Kokubun, “Heterogeneous multi-core fibers: proposal and design principle,” *IEICE Electron. Exp.*, vol. 6, no. 2, pp. 98–103, Jan. 2009.

[21] T. Gonda, K. Imamura, R. Sugizaki, Y. Kawaguchi, T. Tsuritani, “125 μm 5-core fibre with heterogeneous design suitable for migration from single-core system to multi-core system,” *Proc. Eur. Conf. Exhib. Opt. Commun. (ECOC)*, Paper W.2.B.1, Sep. 2016.

[22] P. D. Mcintyre, and A. W. Snyder, “Power transfer between optical fibers,” *J. Opt. Soc. Am.*, vol. 63, no. 12, pp. 1518–1527, 1973.

[23] A. W. Snyder, and A. Ankiewicz, “Optical fiber couplers-optimum solution for unequal cores,” *J. Lightw. Technol.*, vol. 6, no. 3, pp. 463–474, 1988.

[24] H. S. Huang, and H. -C. Chang, “Analysis of optical fiber directional coupling based on the HE_{11} modes-part II: the nonidentical-core case,” *J. Lightw. Technol.*, vol. 8, no. 6, pp. 832–837, Jun. 1990.

[25] K. Okamoto, *Fundamentals of Optical Waveguides*, 2nd ed. (Academic Press. 2006).

[26] J. Tu, K. Saitoh, M. Koshiba, K. Takenaga, and S. Matsuo, “Design and analysis of large-effective-area heterogeneous trench-assisted multi-core fiber,” *Opt. Exp.*, vol. 20, no. 14, pp. 15157–15170, July. 2012.

[27] J. Tu, K. Saitoh, M. Koshiba, K. Takenaga, and S. Matsuo, “Optimized design method for bend-insensitive heterogeneous trench-assisted multi-core fiber with ultra-low crosstalk and high core density,” *J. Lightw. Technol.*, vol. 31, no. 15, pp. 2590–2598, Aug. 2013.

[28] T. Hayashi, T. Taru, O. Shimakawa, T. Sasaki, and E. Sasaoka, “Design and fabrication of ultra-low crosstalk and low-loss multi-core fiber,” *Opt. Exp.*, vol. 19, no. 17, pp. 16576–16592, Aug. 2011.

[29] M. Koshiba, K. Saitoh, K. Takenaga, and S. Matsuo, “Multi-core fiber design and analysis: Coupled-mode theory and coupled-power theory,” *Opt. Exp.*, vol. 19, no. 26, pp. B102–B111, Dec. 2011.

[30] D. Marcuse, “Derivation of coupled power equations,” *Bell Syst. Tech. J.*, vol. 51, no. 1, pp. 229–237, Jan. 1972.

[31] M. Koshiba, K. Saitoh, K. Takenaga, and S. Matsuo, “Analytical expression of average power-coupling coefficients for estimating intercore crosstalk in multicore fibers,” *IEEE Photon. J.*, vol. 4, no. 5, pp. 1987–1995, Oct. 2012.

[32] T. Fujisawa, Y. Amma, Y. Sasaki, S. Matsuo, K. Aikawa, K. Saitoh, and M. Koshiba, “Crosstalk analysis of heterogeneous multicore fibers using coupled-mode theory,” *IEEE Photon. J.*, vol. 9, no. 5, pp. 7204108, Oct. 2017.

[33] T. Hayashi, T. Taru, O. Shimakawa, T. Sasaki, and E. Sasaoka, “Low-crosstalk and low-loss multi-core fiber utilizing fiber bend,” *Proc. Opt. Fiber Commun. Conf. (OFC)*, Paper OWJ3, Mar. 2011.

[34] K. Saitoh, and M. Koshiba, “Full-vectorial imaginary-distance beam propagation method based on a finite element scheme: Application to photonic crystal fibers,” *IEEE J. Quantum Electron.*, vol. 38, no. 7, pp. 927–933, Jul. 2002.

[35] K. Saitoh, “Multi-core fiber technology for SDM: coupling mechanisms and design,” *Proc. Opt. Fiber Commun. Conf. (OFC)*, Paper Tu6B.1, Jun. 2021.

Acknowledgements

First of all, I would like to thank my esteemed supervisor, Professor Kunimasa Saitoh, for his thoughtful supervision and support during my doctoral program in the Graduate School of Information Science and Technology at Hokkaido University. It is a great privilege to spend three years here, and the completion of the Ph.D degree is a big challenge and a good experience for me.

Secondly, I want to express my gratitude to Prof. Takeo Ohgane, Prof. Toshihiko Nishimura, and Assoc. Prof. Takeshi Fujisawa, for their helpful suggestions and guidance in my research work.

I would like to thank all the members in our laboratory, for their kindly help and illuminating suggestions.

Finally, I am also grateful to all my families for their kindly support.

Research achievements

Journals

[1] **Y. Wang**, T. Fujisawa, Y. Sagae, T. Sakamoto, T. Matsui, K. Nakajima, and K. Saitoh, "A Novel Core Allocation in Heterogeneous Step-Index Multi-Core Fibers with Standard Cladding Diameter", IEEE/OSA Journal of Lightwave Technology. (DOI: 10.1109/JLT.2021.3112656)

[2] **Y. Wang**, T. Fujisawa, and K. Saitoh, "Analytical expression for mode-coupling coefficient between non-identical step-index cores and its application to multi-core fiber design within 125-μm cladding diameter", Optics Communications. (DOI: 10.1016/j.optcom.2021.127552)

Conference papers

[1] **Y. Wang**, T. Fujisawa, T. Sakamoto, T. Matsui, K. Nakajima, and K. Saitoh, "Step index 8-core fiber with 125-μm cladding diameter for O-band use", Optoelectronics and Communications Conference (OECC), Paper T3-2.4, Taipei, Taiwan, Oct. 4-8, 2020.

[2] **Y. Wang**, T. Fujisawa, Y. Sagae, T. Sakamoto, T. Matsui, K. Nakajima, and K. Saitoh, "125-μm Cladding Heterogeneous Step-Index Multi-core Fibers for Datacenter Networks", The 6th International Symposium on Extremely Advanced Transmission Technologies (EXAT), Paper P-06, Virtual Conference, November 3-5, 2021.